

# Inverse initial data for nonlinear Schrödinger equation via Carleman estimates and the contraction principle

Navaraj Neupane\*

Loc Nguyen\*

## Abstract

We study an inverse initial-data problem for a nonlinear Schrödinger equation in which the initial wave field is reconstructed from lateral measurements. Our approach combines a Legendre-polynomial-exponential-time dimensional reduction with a Carleman-based contraction principle. First, we expand the solution in a weighted Legendre basis in time and truncate the expansion to obtain a coupled nonlinear elliptic system for the spatial coefficients. Next, we solve this reduced system by constructing a contraction map on a suitable admissible set. This contraction map admits a unique fixed point, which is the limit of the corresponding Picard iteration. We also establish a stability estimate showing that this fixed point remains close to the exact reduced solution in the noisy-data case. Finally, we present numerical experiments in two space dimensions for several different geometries and nonlinear exponents. The numerical results show that the proposed method accurately reconstructs the main features of the initial wave field and remains stable even when the boundary data contain noise.

**Keywords:** nonlinear Schrödinger equation; inverse initial-data problem; Carleman estimate; time-dimensional reduction; Legendre polynomial-exponential basis; contraction mapping; Picard iteration; noisy boundary data.

**MSC 2020:** 35R30, 35Q55, 35J57, 35B45, 65N21.

## 1 Introduction

Let  $d \geq 1$  be the spatial dimension, let  $\Omega$  be a bounded domain of  $\mathbb{R}^d$  with smooth boundary, and let  $T > 0$  be a final time. We consider the nonlinear Schrödinger equation

$$\begin{cases} iu_t + \Delta u + q(\mathbf{x}, t)|u|^{p-1}u = 0, & \text{in } \Omega \times (0, T), \\ u(\mathbf{x}, t) = 0, & \text{on } \partial\Omega \times (0, T), \\ u(\mathbf{x}, 0) = u^0(\mathbf{x}), & \text{in } \Omega, \end{cases} \quad (1.1)$$

where  $u : \Omega \times (0, T) \rightarrow \mathbb{C}$  is the wave field and  $u^0 : \Omega \rightarrow \mathbb{C}$  is the initial wave field. The function  $q(\mathbf{x}, t)$  is a given real-valued coefficient describing the strength of the nonlinear interaction, and  $p > 1$  is the exponent of the nonlinearity. In particular,  $p = 2$ ,  $p = 3$ , and  $p = 5$  correspond to quadratic, cubic, and quintic nonlinear Schrödinger models, respectively. Among these, the cubic case  $p = 3$  is the most classical and widely studied, especially in nonlinear optics, Bose–Einstein condensation, and wave propagation in dispersive media. Moreover, if  $q \in L^\infty(\Omega \times (0, T))$  and  $u^0 \in H_0^1(\Omega)$ , then the forward problem (1.1) is locally well-posed for any finite  $p > 1$  when  $d = 1, 2$ , whereas for  $d \geq 3$  one works in the range  $1 < p \leq 1 + \frac{4}{d-2}$ ; see, for instance, [12, 47].

Assuming that (1.1) has a unique solution, we are interested in the following inverse problem.

---

\*Department of Mathematics and Statistics, University of North Carolina at Charlotte, Charlotte, NC 28223, USA (nneupan2@charlotte.edu loc.nguyen@charlotte.edu).

**Problem 1.1** (Inverse initial-data problem). *Given the lateral Neumann data*

$$f(\mathbf{x}, t) = \partial_\nu u(\mathbf{x}, t) \quad \text{for all } (\mathbf{x}, t) \in \partial\Omega \times (0, T), \quad (1.2)$$

*reconstruct the initial wave field  $u^0(\mathbf{x})$  for  $\mathbf{x} \in \Omega$ .*

This inverse problem is significant from both practical and mathematical points of view. Nonlinear Schrödinger equations arise in many applications, including nonlinear optics, Bose–Einstein condensation, plasma physics, and deep-water wave propagation [36, 44, 47, 50]. In such settings, the initial wave field contains essential information about the state of the system at the initial time, but direct interior measurements are often difficult or impossible to obtain. By contrast, boundary observations are more accessible in experiments and monitoring processes. Therefore, recovering  $u^0$  from lateral Neumann data provides a useful noninvasive way to identify the hidden initial state of the system. Once  $u^0$  is reconstructed, the full wave field can then be recovered by solving the forward problem (1.1).

Inverse problems for Schrödinger equations have been studied extensively over the past several decades. Early works focused mainly on the recovery of electric potentials, coefficients, and magnetic fields from boundary measurements [5, 7, 8, 13, 18, 19]. In the linear Schrödinger setting, representative contributions include inverse potential recovery results under degenerate weights [37], problems with discontinuous and variable coefficients [3, 17], magnetic and electromagnetic inverse problems in bounded and cylindrical geometries [5, 6, 7, 9, 10, 14, 20, 23], and a Neumann-boundary formulation [46]. More recently, inverse problems for nonlinear Schrödinger equations and partial boundary data have also attracted considerable attention. Uniqueness for nonlinear magnetic Schrödinger equations on conformally transversally anisotropic manifolds was established in [27]. Partial-data inverse problems for nonlinear magnetic Schrödinger equations were studied in [29], while partial-data determination of a time-dependent nonlinear coefficient was obtained in [28]. Stable determination of coefficients in nonlinear dynamical Schrödinger equations from Neumann data was investigated in [2]. These works form the main historical background for the present study. A conventional numerical approach to nonlinear inverse problems is to formulate a least-squares discrepancy functional and minimize it by an iterative optimization procedure. Such methods can be effective, but they often depend strongly on the choice of initial guess and may converge slowly or become trapped in undesirable local minima when the initial approximation is poor. In contrast, our approach begins by eliminating the time variable through a Legendre polynomial-exponential expansion and truncating the solution to the first  $N + 1$  modes. This reduces the original inverse problem to a coupled nonlinear elliptic system for the spatial coefficients. We then solve the reduced system by a Carleman–Picard strategy: at each iteration, the nonlinear term is frozen at the current approximation, and the next iterate is defined as the unique minimizer of a Carleman-weighted regularized functional. This procedure generates a contraction map on a suitable admissible set, and hence the Picard iteration converges from an arbitrary initial guess to a unique fixed point. The approximate initial wave field is finally reconstructed by evaluating the truncated expansion at  $t = 0$ .

The methodological background of the present paper comes from the combination of time-dimensional reduction and the Carleman contraction principle. This approach was first developed in [34] for an inverse initial-value problem for a quasilinear parabolic equation. Later, [41] showed that the method can be interpreted as the construction of a contraction mapping whose fixed point is the desired solution. Consequently, the associated Picard iteration converges globally, even when the initial guess is far from the true solution. Since then, this framework has been extended to a variety of inverse problems; see, for example, [1, 15, 31, 33, 38, 42, 43, 49], in which inverse problems for hyperbolic, parabolic, elliptic, elasticity and Navier-Stokes equations were investigated.

Nevertheless, these earlier results, which require a Lipschitz condition imposed on the nonlinearity, cannot be applied directly to the present problem because of the  $p$ -growth nonlinearity in (1.1). After the time-dimensional reduction, the reduced system contains nonlinear terms of the form

$$\left| \sum_{\ell=0}^N u_{\ell}(\mathbf{x}) \Psi_{\ell}(t) \right|^{p-1} \left( \sum_{\ell=0}^N u_{\ell}(\mathbf{x}) \Psi_{\ell}(t) \right),$$

which induce nonlinear coupling among all reduced modes and do not satisfy the structural assumptions imposed on the nonlinearities in [34, 41]. Therefore, a new adaptation of the Carleman contraction framework is required for the nonlinear Schrödinger equation.

The main contribution of this paper is to develop a Carleman contraction method for the inverse initial-data problem for the nonlinear Schrödinger equation. More precisely, we construct a contraction map on a suitable admissible set for the time-dimensional reduction model and prove that its unique fixed point can be obtained by a globally convergent Picard iteration. We then show that this fixed point is consistent with the exact reduced solution. In the noisy-data case, we establish a stability estimate showing that the fixed point remains close to the exact reduced solution, with the reconstruction error controlled by the noise level and the regularization parameter. Unlike several standard Carleman-based frameworks, our noise estimate does not require any special structural condition on the noise.

The remainder of the paper is organized as follows. Section 2 recalls the analytical tools needed later, including the relevant Carleman estimate and the properties of the Legendre polynomial-exponential basis. Section 3 derives the time-dimensional reduction model and the reduced boundary data. Section 4 develops the Carleman-based contraction principle for the reduced system. Section 5 proves the consistency of the fixed point with the exact reduced solution. Section 6 presents the numerical algorithm and computational examples. Section 7 is for the concluding remarks.

## 2 Preliminary analytical tools

This section presents the main analytical ingredients used throughout the paper. First, we recall a Carleman estimate for an elliptic operator in divergence form, which will be used later in the analysis of the reduced system. Next, we summarize the basic properties of the Legendre polynomial-exponential basis underlying our time-dimensional reduction method. For the reader's convenience, we also include a convergence result for the expansion of the first-time derivative.

### 2.1 A Carleman estimate

A key tool in our analysis is a Carleman estimate for an elliptic operator in divergence form. Let

$$A : \bar{\Omega} \rightarrow \mathbb{R}^{d \times d}$$

be a matrix-valued function of class  $C^2(\bar{\Omega})$ . Assume that

1.  $A$  is symmetric, that is,

$$A^T = A;$$

2.  $A$  is uniformly elliptic: there exists a constant  $\Lambda > 0$  such that

$$\Lambda^{-1} |\xi|^2 \leq A(\mathbf{x}) \xi \cdot \xi \leq \Lambda |\xi|^2 \quad \text{for all } \mathbf{x} \in \bar{\Omega}, \xi \in \mathbb{R}^d. \quad (2.1)$$

Let  $\mathbf{x}_0 \in \mathbb{R}^d \setminus \overline{\Omega}$  and define

$$r(\mathbf{x}) = |\mathbf{x} - \mathbf{x}_0|, \quad \mathbf{x} \in \overline{\Omega}.$$

Also, let

$$R = \max_{\mathbf{x} \in \overline{\Omega}} r(\mathbf{x}).$$

**Lemma 2.1.** *Let  $u \in C^2(\overline{\Omega})$ . Then there exists a constant  $\beta_0 > 0$ , depending only on  $\|A\|_{C^1(\overline{\Omega})}$  and  $\Lambda$ , such that for every  $\beta \geq \beta_0$  and every  $\lambda \geq \lambda_0 := 2R^\beta$ ,*

$$r^{\beta+2} e^{2\lambda r^{-\beta}} |\operatorname{div}(A\nabla u)|^2 \geq C \left[ \operatorname{div}(U) + \lambda^3 \beta^4 e^{2\lambda r^{-\beta}} r^{-2\beta-2} |u|^2 + \lambda \beta e^{2\lambda r^{-\beta}} |\nabla u|^2 \right] \quad (2.2)$$

in  $\Omega$ , where  $U$  is a vector-valued function satisfying

$$|U| \leq C e^{2\lambda r^{-\beta}} (\lambda^3 \beta^3 r^{-2\beta-2} |u|^2 + \lambda \beta |\nabla u|^2), \quad (2.3)$$

and where  $C > 0$  depends only on  $\mathbf{x}_0$ ,  $\Omega$ ,  $\|A\|_{C^1(\overline{\Omega})}$ ,  $\Lambda$ , and  $d$ .

The proof is based on the behavior of the exponential weight  $e^{\lambda r^{-\beta}}$ . The main task is to estimate the quantity

$$e^{2\lambda r^{-\beta}} |\operatorname{div}(A\nabla u)|^2.$$

To do so, one applies the product rule to the weighted operator. In the course of this computation, the second derivatives of  $u$  are redistributed into terms involving first-order derivatives and zeroth-order terms. At the same time, each differentiation of the exponential weight produces a factor containing the large parameter  $\lambda$ . As a result, after expanding the weighted operator, one obtains dominant positive terms with high powers of  $\lambda$ , as seen in (2.2). We omit the proof here and refer the reader to [32] for the full details.

A convenient consequence of Lemma 2.1 is the following simplified form.

**Corollary 2.1.** *Fix  $\beta \geq \beta_0$ . Then there exists a constant  $\lambda_0 > 0$ , depending only on  $\Lambda$ ,  $\|A\|_{C^2(\overline{\Omega})}$ ,  $\mathbf{x}_0$ ,  $\Omega$ ,  $R$ ,  $\beta$ , and  $d$ , such that for all  $\lambda \geq \lambda_0$ ,*

$$e^{2\lambda r^{-\beta}} |\operatorname{div}(A\nabla u)|^2 \geq C \left[ \operatorname{div}(U) + \lambda^3 e^{2\lambda r^{-\beta}} |u|^2 + \lambda e^{2\lambda r^{-\beta}} |\nabla u|^2 \right] \quad (2.4)$$

in  $\Omega$ , where  $C > 0$  depends only on  $\Lambda$ ,  $\|A\|_{C^2(\overline{\Omega})}$ ,  $\mathbf{x}_0$ ,  $\Omega$ ,  $R$ ,  $\beta$ , and  $d$ .

Integrating (2.4) over  $\Omega$  and using (2.3), we obtain the following global form.

**Corollary 2.2.** *There exists a constant  $C > 0$ , depending only on  $\Lambda$ ,  $\|A\|_{C^2(\overline{\Omega})}$ ,  $\mathbf{x}_0$ ,  $\Omega$ ,  $R$ ,  $\beta$ , and  $d$ , such that*

$$\begin{aligned} \int_{\Omega} e^{2\lambda r^{-\beta}} |\operatorname{div}(A\nabla u)|^2 d\mathbf{x} &\geq C \int_{\Omega} e^{2\lambda r^{-\beta}} [\lambda^3 |u|^2 + \lambda |\nabla u|^2] d\mathbf{x} \\ &\quad - C \int_{\partial\Omega} e^{2\lambda r^{-\beta}} [\lambda^3 |u|^2 + \lambda |\nabla u|^2] d\sigma(\mathbf{x}). \end{aligned} \quad (2.5)$$

In particular, if

$$u|_{\partial\Omega} = 0 \quad \text{and} \quad \nabla u|_{\partial\Omega} = 0,$$

then

$$\int_{\Omega} e^{2\lambda r^{-\beta}} |\operatorname{div}(A\nabla u)|^2 d\mathbf{x} \geq C \int_{\Omega} e^{2\lambda r^{-\beta}} [\lambda^3 |u|^2 + \lambda |\nabla u|^2] d\mathbf{x}. \quad (2.6)$$

**Remark 2.1.** Estimate (2.5) is closely related to [39, Lemma 5]. The main difference is that the result in [39, Lemma 5] was established for annular domains, whereas (2.5) is valid for more general bounded domains. It is worth mentioning that the Carleman estimate in [39, Lemma 5] was used there to prove a cloaking phenomenon. The reader can find many other variants of Carleman estimates in [4, 24, 25, 40, 45]. Such estimates have become an essential tool in the study of inverse problems; see, for example, [22, 34, 38].

**Corollary 2.3.** Assume that  $A = I$ , the identity matrix. Then  $\operatorname{div}(A\nabla u) = \Delta u$ , and Corollary 2.2 yields the following estimate

$$\int_{\Omega} e^{2\lambda r^{-\beta}} |\Delta u|^2 \, d\mathbf{x} \geq C \int_{\Omega} e^{2\lambda r^{-\beta}} [\lambda^3 |u|^2 + \lambda |\nabla u|^2] \, d\mathbf{x} - C \int_{\partial\Omega} e^{2\lambda r^{-\beta}} [\lambda^3 |u|^2 + \lambda |\nabla u|^2] \, d\sigma(\mathbf{x}). \quad (2.7)$$

In particular, if  $u|_{\partial\Omega} = 0$  then  $|\nabla u| = |\partial_{\nu} u|$ . In this case, (2.7) becomes

$$\int_{\Omega} e^{2\lambda r^{-\beta}} |\Delta u|^2 \, d\mathbf{x} \geq C \int_{\Omega} e^{2\lambda r^{-\beta}} [\lambda^3 |u|^2 + \lambda |\nabla u|^2] \, d\mathbf{x} - C \int_{\partial\Omega} e^{2\lambda r^{-\beta}} \lambda |\partial_{\nu} u|^2 \, d\sigma(\mathbf{x}). \quad (2.8)$$

## 2.2 The Legendre polynomial-exponential basis

Our time-dimensional reduction method is based on the Legendre polynomial-exponential basis introduced in [48]; see also [49] for related properties used in the reduction process. For the reader's convenience, we briefly summarize the main definitions and facts needed later.

Let  $\{P_n\}_{n \geq 0}$  be the classical Legendre polynomials on  $(-1, 1)$ , given by Rodrigues' formula

$$P_n(x) = \frac{1}{2^n n!} \frac{d^n}{dx^n} (x^2 - 1)^n.$$

To transfer this family to the interval  $(0, T)$ , we use the affine change of variables

$$x = \frac{2t}{T} - 1,$$

and define

$$Q_n(t) := \sqrt{\frac{2n+1}{T}} P_n\left(\frac{2t}{T} - 1\right), \quad t \in (0, T), \quad n \geq 0.$$

Then  $\{Q_n\}_{n \geq 0}$  is an orthonormal basis of  $L^2(0, T)$ .

Following [48], we introduce the weighted functions

$$\Psi_n(t) := e^t Q_n(t), \quad t \in (0, T), \quad n \geq 0.$$

The family  $\{\Psi_n\}_{n \geq 0}$  is orthonormal with respect to the weighted inner product

$$\langle u, v \rangle_{e^{-2t}} := \int_0^T e^{-2t} u(t) v(t) \, dt,$$

and therefore forms an orthonormal basis in the weighted space

$$L_{e^{-2t}}^2(0, T) := \left\{ u \in L^2(0, T) : \int_0^T e^{-2t} |u(t)|^2 \, dt < \infty \right\}.$$

**Remark 2.2.** The weighted space  $L_{e^{-2t}}^2(0, T)$  coincides with the classical space  $L^2(0, T)$ , since the weight  $e^{-2t}$  is positive and bounded above and below on the finite interval  $(0, T)$ . In particular, the corresponding norms are equivalent. We use the notation  $L_{e^{-2t}}^2(0, T)$  in order to emphasize the presence of the weight  $e^{-2t}$  in the associated inner product and norm.

We next recall several properties of this basis that will be used throughout the paper.

**Proposition 2.1** (See [48]). *The Legendre polynomial-exponential basis functions  $\Psi_n$ ,  $n \geq 0$ , satisfy the following properties.*

1. For each  $n \geq 0$ , the function  $\Psi_n$  is infinitely differentiable on  $(0, T)$ , and none of its derivatives of any order vanishes identically on this interval.
2. For every integer  $\ell \in \mathbb{N}$ , there exists a constant  $C > 0$ , depending only on  $\ell$  and  $T$ , such that for all  $u \in H^\ell(0, T)$ ,

$$\sum_{n=0}^{\infty} n^{2\ell} |\langle u, \Psi_n \rangle_{e^{-2t}}|^2 \leq C \|u\|_{H^\ell(0, T)}^2. \quad (2.9)$$

3. There exists a constant  $C > 0$ , depending only on  $T$ , such that for all  $n \geq 1$ ,

$$\|\Psi_n'\|_{L_{e^{-2t}}^2(0, T)} \leq Cn^{3/2}, \quad \|\Psi_n''\|_{L_{e^{-2t}}^2(0, T)} \leq Cn^{7/2}. \quad (2.10)$$

**Remark 2.3.** The statements in Proposition 2.1 follow from the results established in [48]; see in particular Proposition 2.1, Lemma 2.1, and Lemma 2.2 there. The exponential factor in the definition  $\Psi_n = e^t Q_n$  plays an important role. Indeed, without this factor, some time modes would have derivatives that vanish identically, which is undesirable in the time-reduction procedure.

The next proposition provides the counterpart, at the level of the first time derivative, of the second-derivative convergence result established in [48].

**Proposition 2.2.** *Let  $p \geq 0$  and assume that*

$$u \in H^\ell((0, T); H^p(\Omega)) \quad \text{for some } \ell \geq 3.$$

Denote the Legendre-exponential coefficients of  $u$  by

$$u_n(\cdot) := \langle u(\cdot, \cdot), \Psi_n \rangle_{L_{e^{-2t}}^2(0, T)} = \int_0^T e^{-2t} u(\cdot, t) \Psi_n(t) dt, \quad n \geq 0.$$

Then  $u_t \in L^2((0, T); H^p(\Omega))$  and

$$\partial_t u(\cdot, t) = \sum_{n=0}^{\infty} u_n(\cdot) \Psi_n'(t) \quad \text{in } L^2((0, T); H^p(\Omega)).$$

**Remark 2.4.** The proof of Proposition 2.2 follows the same line of argument as the proof of the corresponding second-derivative result in [48]. The condition  $\ell \geq 3$  comes from combining the coefficient decay estimate (2.9) with the derivative bound (2.10); see also [49, Theorem 1] for further details.

### 3 The time-dimensional reduction model

Let  $\{\Psi_n\}_{n \geq 0}$  be the Legendre exponential-polynomial basis of  $L^2(0, T)$ , introduced in [48]. We write

$$u(\mathbf{x}, t) = \sum_{n=0}^{\infty} u_n(\mathbf{x}) \Psi_n(t) \quad \text{for } (\mathbf{x}, t) \in \Omega \times (0, T), \quad (3.1)$$

where

$$u_n(\mathbf{x}) = \int_0^T e^{-2t} u(\mathbf{x}, t) \Psi_n(t) dt.$$

By Proposition 2.2, see also [49, Theorem 1],

$$u_t(\mathbf{x}, t) = \sum_{n=0}^{\infty} u_n(\mathbf{x}) \Psi'_n(t) \quad \text{for } (\mathbf{x}, t) \in \Omega \times (0, T). \quad (3.2)$$

Plugging (3.1) and (3.2) into the Schrödinger equation (1.1), we obtain

$$i \sum_{n=0}^{\infty} u_n(\mathbf{x}) \Psi'_n(t) + \sum_{n=0}^{\infty} \Delta u_n(\mathbf{x}) \Psi_n(t) + q(\mathbf{x}, t) \left| \sum_{l=0}^{\infty} u_l(\mathbf{x}) \Psi_l(t) \right|^{p-1} \sum_{n=0}^{\infty} u_n(\mathbf{x}) \Psi_n(t) = 0 \quad (3.3)$$

for  $(\mathbf{x}, t) \in \Omega \times (0, T)$ .

For each  $m \geq 0$ , multiply both sides of (3.3) by  $e^{-2t} \Psi_m(t)$  and integrate over  $t \in (0, T)$ . Using the orthonormality relation

$$\int_0^T e^{-2t} \Psi_n(t) \Psi_m(t) dt = \delta_{mn},$$

and denoting

$$\mathbf{u} = [u_0 \quad u_1 \quad \dots]^\top,$$

we obtain

$$i \sum_{n=0}^{\infty} s_{mn} u_n(\mathbf{x}) + \Delta u_m(\mathbf{x}) + \sum_{n=0}^{\infty} b_{mn}(\mathbf{u}, \mathbf{x}) u_n(\mathbf{x}) = 0, \quad (3.4)$$

where

$$s_{mn} = \int_0^T e^{-2t} \Psi'_n(t) \Psi_m(t) dt, \quad (3.5)$$

$$b_{mn}(\mathbf{u}, \mathbf{x}) = \int_0^T e^{-2t} q(\mathbf{x}, t) \left| \sum_{l=0}^{\infty} u_l(\mathbf{x}) \Psi_l(t) \right|^{p-1} \Psi_n(t) \Psi_m(t) dt. \quad (3.6)$$

Fix a cutoff number  $N \geq 0$ . By truncating the series in (3.4), we approximate it by

$$i \sum_{n=0}^N s_{mn} u_n(\mathbf{x}) + \Delta u_m(\mathbf{x}) + \sum_{n=0}^N b_{mn}^N(\mathbf{u}^N, \mathbf{x}) u_n(\mathbf{x}) = 0, \quad m = 0, 1, \dots, N, \quad (3.7)$$

where

$$\mathbf{u}^N = [u_0 \quad u_1 \quad \dots \quad u_N]^\top, \quad (3.8)$$

$$b_{mn}^N(\mathbf{u}^N, \mathbf{x}) = \int_0^T e^{-2t} q(\mathbf{x}, t) \left| \sum_{l=0}^N u_l(\mathbf{x}) \Psi_l(t) \right|^{p-1} \Psi_n(t) \Psi_m(t) dt. \quad (3.9)$$

Equation (3.7) serves as the time-dimensional reduction model, which approximates the original time-dependent Schrödinger equation. We next compute the boundary conditions for  $u_m$ .

Using (3.1) and the homogeneous Dirichlet boundary condition in (1.1), we have

$$\sum_{n=0}^{\infty} u_n(\mathbf{x}) \Psi_n(t) = 0 \quad \text{for } (\mathbf{x}, t) \in \partial\Omega \times (0, T).$$

Multiplying both sides by  $e^{-2t} \Psi_m(t)$  and integrating over  $(0, T)$ , we obtain

$$u_m(\mathbf{x}) = 0 \quad \text{for } \mathbf{x} \in \partial\Omega, \quad m \geq 0. \quad (3.10)$$

Next, differentiating (3.1) in the outward normal direction yields

$$\partial_\nu u(\mathbf{x}, t) = \sum_{n=0}^{\infty} \partial_\nu u_n(\mathbf{x}) \Psi_n(t) \quad \text{for } (\mathbf{x}, t) \in \partial\Omega \times (0, T).$$

Using the Neumann data (1.2), we obtain

$$f(\mathbf{x}, t) = \sum_{n=0}^{\infty} \partial_\nu u_n(\mathbf{x}) \Psi_n(t) \quad \text{for } (\mathbf{x}, t) \in \partial\Omega \times (0, T).$$

Multiplying both sides by  $e^{-2t} \Psi_m(t)$  and integrating over  $(0, T)$ , we arrive at

$$\partial_\nu u_m(\mathbf{x}) = f_m(\mathbf{x}) \quad \text{for } \mathbf{x} \in \partial\Omega, \quad m \geq 0, \quad (3.11)$$

where

$$f_m(\mathbf{x}) := \int_0^T e^{-2t} f(\mathbf{x}, t) \Psi_m(t) dt. \quad (3.12)$$

Hence, for each  $m = 0, 1, \dots, N$ , the function  $u_m$  satisfies the boundary conditions (3.10) and (3.11) on  $\partial\Omega$ . Therefore, combining (3.7), (3.10), and (3.11), we obtain the following coupled elliptic system:

$$\begin{cases} i \sum_{n=0}^N s_{mn} u_n(\mathbf{x}) + \Delta u_m(\mathbf{x}) + \sum_{n=0}^N b_{mn}^N(\mathbf{u}^N, \mathbf{x}) u_n(\mathbf{x}) = 0, & \mathbf{x} \in \Omega, \\ u_m(\mathbf{x}) = 0, & \mathbf{x} \in \partial\Omega, \\ \partial_\nu u_m(\mathbf{x}) = f_m(\mathbf{x}), & \mathbf{x} \in \partial\Omega, \end{cases} \quad m = 0, 1, \dots, N. \quad (3.13)$$

Solving system (3.13) is the next step of our method.

**Remark 3.1.** *System (3.13) will be referred to as the **time-dimensional reduction model**. It provides an approximate reduction of the original time-dependent Schrödinger problem by eliminating the explicit time variable through the truncated expansion (3.1). As a result, instead of working on the  $(d+1)$ -dimensional space-time domain  $\Omega \times (0, T)$ , one only needs to solve a coupled system on the  $d$ -dimensional spatial domain  $\Omega$ . This reduction significantly decreases the computational cost.*

*In addition, the derivation of (3.13) involves truncating the expansion to the first  $N+1$  modes. Therefore, the high-oscillation components of the data are discarded. This truncation acts as a filtering step and can help reduce the influence of noise in practical computations.*

## 4 A Carleman-contraction principle for the time-dimensional reduction model

Let  $s > \frac{d}{2} + 2$ . Then, by the Sobolev embedding theorem,

$$H^s(\Omega) \hookrightarrow C^2(\overline{\Omega}),$$

and in particular

$$H^s(\Omega) \hookrightarrow L^\infty(\Omega).$$

Moreover, the mappings

$$u \mapsto \Delta u, \quad u \mapsto u|_{\partial\Omega}, \quad u \mapsto \partial_\nu u|_{\partial\Omega}$$

are continuous from  $H^s(\Omega)$  into  $L^2(\Omega)$ ,  $L^2(\partial\Omega)$ , and  $L^2(\partial\Omega)$ , respectively. We seek a solution to (3.13) in the admissible set

$$H = \left\{ \boldsymbol{\varphi} \in [H^s(\Omega)]^{N+1} : \boldsymbol{\varphi}|_{\partial\Omega} = \mathbf{0} \text{ and } \|\boldsymbol{\varphi}\|_{[L^\infty(\Omega)]^{N+1}} \leq M \right\},$$

where  $M > 0$  is a fixed constant chosen sufficiently large.

**Remark 4.1.** *The restriction to the admissible set  $H$  is imposed as an a priori regularity assumption on the exact coefficient vector. More precisely, we assume that the exact coefficient vector belongs to  $[H^s(\Omega)]^{N+1}$ . Hence, for  $M$  sufficiently large, it belongs to  $H$ . Therefore,  $H$  should be viewed as a natural class of physically meaningful solutions rather than as a restrictive assumption.*

Fix  $\beta \geq \beta_0$  where  $\beta_0$  is as in Lemma 2.1. For each  $\lambda > \lambda_0$ , where  $\lambda_0$  is also defined in Lemma 2.1, and  $\epsilon > 0$ , for each  $\boldsymbol{\varphi} = [\varphi_0 \ \varphi_1 \ \dots \ \varphi_N]^\top \in H$ , define

$$J_{\boldsymbol{\varphi}}^{\lambda, \epsilon}(\mathbf{u}) := \sum_{m=0}^N \left[ \int_{\Omega} e^{2\lambda r^{-\beta}} \left| i \sum_{n=0}^N s_{mn} u_n(\mathbf{x}) + \Delta u_m(\mathbf{x}) + \sum_{n=0}^N b_{mn}^N(\boldsymbol{\varphi}, \mathbf{x}) \varphi_n(\mathbf{x}) \right|^2 dx + \lambda^3 \int_{\partial\Omega} e^{2\lambda r^{-\beta}} |\partial_\nu u_m - f_m|^2 d\sigma(\mathbf{x}) + \epsilon \|u_m\|_{H^s(\Omega)}^2 \right]. \quad (4.1)$$

**Proposition 4.1.** *Given  $\lambda > \lambda_0$  and  $\epsilon > 0$ , the functional  $J_{\boldsymbol{\varphi}}^{\lambda, \epsilon}$  admits a unique minimizer on  $H$  for every  $\boldsymbol{\varphi} \in H$ .*

*Proof.* The existence of a minimizer follows from the direct method in the calculus of variations; see, for example, [16, 51]. Fix  $\boldsymbol{\varphi} \in H$ . Clearly,  $H$  is nonempty, since  $0 \in H$ . In addition, the continuity of the embedding  $H^s(\Omega) \hookrightarrow L^\infty(\Omega)$  implies that  $H$  is a closed and convex subset of  $[H^s(\Omega)]^{N+1}$ . Since  $[H^s(\Omega)]^{N+1}$  is a Hilbert space,  $H$  is also weakly closed.

Since  $\boldsymbol{\varphi} \in H$  and  $q \in L^\infty(\Omega \times (0, T))$ , we have  $b_{mn}^N(\boldsymbol{\varphi}, \cdot) \in L^\infty(\Omega)$  for all  $m, n = 0, \dots, N$ . Moreover, since  $s > \frac{d}{2} + 2$ , the operators  $\Delta$ , the Dirichlet trace, and the Neumann trace are continuous on  $H^s(\Omega)$ . Also, since  $\mathbf{x}_0 \notin \overline{\Omega}$ , the function  $r(\mathbf{x}) = |\mathbf{x} - \mathbf{x}_0|$  is bounded above and below by positive constants on  $\overline{\Omega}$ . Hence the weight  $e^{2\lambda r^{-\beta}}$  is bounded above and below by positive constants on  $\Omega$  and on  $\partial\Omega$ . Therefore,  $J_{\boldsymbol{\varphi}}^{\lambda, \epsilon}$  is well defined on  $H$ .

We first prove the existence of a minimizer. Since every term in  $J_{\boldsymbol{\varphi}}^{\lambda, \epsilon}$  is nonnegative,

$$J_{\boldsymbol{\varphi}}(\mathbf{u}) \geq \epsilon \sum_{m=0}^N \|u_m\|_{H^s(\Omega)}^2 = \epsilon \|\mathbf{u}\|_{[H^s(\Omega)]^{N+1}}^2 \quad \text{for all } \mathbf{u} \in H.$$

Thus  $J_\varphi^{\lambda,\epsilon}$  is coercive on  $H$ . Let  $\alpha := \inf_{\mathbf{u} \in H} J_\varphi^{\lambda,\epsilon}(\mathbf{u})$ , and let  $\{\mathbf{u}^k\}_{k=1}^\infty \subset H$  be a minimizing sequence such that  $J_\varphi^{\lambda,\epsilon}(\mathbf{u}^k) \rightarrow \alpha$  as  $k \rightarrow \infty$ . By coercivity,  $\{\mathbf{u}^k\}_{k=1}^\infty$  is bounded in  $[H^s(\Omega)]^{N+1}$ . Since  $[H^s(\Omega)]^{N+1}$  is a Hilbert space, there exist a subsequence, still denoted by  $\{\mathbf{u}^k\}_{k=1}^\infty$ , and an element  $\mathbf{u}^* \in [H^s(\Omega)]^{N+1}$  such that

$$\mathbf{u}^k \rightharpoonup \mathbf{u}^* \quad \text{weakly in } [H^s(\Omega)]^{N+1}.$$

Because  $H$  is weakly closed, we have  $\mathbf{u}^* \in H$ .

The operators  $\Delta$ , the Dirichlet trace, and the Neumann trace are continuous and linear with respect to  $\mathbf{u}$ . Therefore, under the weak convergence above, the corresponding images converge weakly in their target spaces. It follows from the weak lower semicontinuity of the norm that

$$J_\varphi^{\lambda,\epsilon}(\mathbf{u}^*) \leq \liminf_{k \rightarrow \infty} J_\varphi^{\lambda,\epsilon}(\mathbf{u}^k) = \alpha.$$

Hence  $\mathbf{u}^*$  is a minimizer of  $J_\varphi^{\lambda,\epsilon}$  on  $H$ . The uniqueness of the minimizer follows from the strict convexity of  $J_\varphi^{\lambda,\epsilon}$  on the convex set  $H$ .  $\square$

Define  $F_{\lambda,\epsilon} : H \rightarrow H$  by letting  $F(\varphi)$  be the unique minimizer of  $J_\varphi^{\lambda,\epsilon}$  on  $H$ , that is,

$$F_{\lambda,\epsilon}(\varphi) := \operatorname{argmin}_{\mathbf{u} \in H} J_\varphi^{\lambda,\epsilon}(\mathbf{u}).$$

The well-definedness of  $F_{\lambda,\epsilon}$  follows from Proposition 4.1. We next show that when  $\lambda$  is sufficiently large, the map  $F_{\lambda,\epsilon}$  is contractive with respect to the norm

$$\|\mathbf{u}\|_{\lambda,\epsilon}^2 = \int_{\Omega} e^{2\lambda r^{-\beta}} |\mathbf{u}|^2 d\mathbf{x} + 2 \int_{\partial\Omega} e^{2\lambda r^{-\beta}} |\partial_\nu \mathbf{u}|^2 d\sigma(\mathbf{x}) + \frac{2\epsilon}{\lambda^3} \|\mathbf{u}\|_{[H^s(\Omega)]^{N+1}}^2 \quad (4.2)$$

**Theorem 4.1.** *Let  $\epsilon > 0$ . Fix  $\beta > \beta_0$ . There exist  $\lambda_1$  and  $C$  depending only on  $\Omega$ ,  $\beta$ ,  $s$ ,  $N$ ,  $p$ ,  $T$ ,  $\|q\|_{L^\infty(\Omega \times (0,T))}$ ,  $\{\Psi_\ell\}_{\ell=0}^N$ ,  $\{s_{mn}\}_{m,n=0}^N$ , and  $M$  such that for all  $\lambda > \lambda_1$ , we have*

$$\|F_{\lambda,\epsilon}(\varphi) - F_{\lambda,\epsilon}(\psi)\|_{\lambda,\epsilon} \leq \sqrt{\frac{C}{\lambda^3}} \|\varphi - \psi\|_{\lambda,\epsilon} \quad (4.3)$$

for all  $\varphi$  and  $\psi$  in  $H$ .

*Proof.* Throughout the proof,  $C > 0$  denotes a generic constant depending only on the parameters in the statement of the theorem. The constant  $C$  might vary from estimate to estimate.

Let  $\varphi = [\varphi_0 \ \dots \ \varphi_N]^\top$  and  $\psi = [\psi_0 \ \dots \ \psi_N]^\top$  be two vector-valued functions in  $H$ . Set

$$\mathbf{u} = F_{\lambda,\epsilon}(\varphi), \quad \mathbf{v} = F_{\lambda,\epsilon}(\psi), \quad \text{and} \quad \mathbf{h} = \mathbf{u} - \mathbf{v}.$$

Since  $H$  is convex, for all  $\theta \in (0, 1)$ ,

$$\theta \mathbf{v} + (1 - \theta) \mathbf{u} = \mathbf{u} - \theta(\mathbf{u} - \mathbf{v}) = \mathbf{u} - \theta \mathbf{h} \in H.$$

Since  $\mathbf{u}$  is the minimizer of  $J_\varphi^{\lambda,\epsilon}$ , for all  $\theta \in (0, 1)$ , writing

$$\mathbf{u} = [u_0 \ \dots \ u_N]^\top \quad \text{and} \quad \mathbf{v} = [v_0 \ \dots \ v_N]^\top$$

gives

$$\begin{aligned}
0 &\leq \frac{J_{\varphi}^{\lambda, \epsilon}(\mathbf{u} - \theta \mathbf{h}) - J_{\varphi}^{\lambda, \epsilon}(\mathbf{u})}{\theta} \\
&= \frac{1}{\theta} \sum_{m=0}^N \left[ \left\| e^{\lambda r^{-\beta}} \left( i \sum_{n=0}^N s_{mn} (u_n - \theta h_n) + \Delta(u_m - \theta h_m) + \sum_{n=0}^N b_{mn}^N(\varphi, \mathbf{x}) \varphi_n \right) \right\|_{L^2(\Omega)}^2 \right. \\
&\quad - \left\| e^{\lambda r^{-\beta}} \left( i \sum_{n=0}^N s_{mn} u_n + \Delta u_m + \sum_{n=0}^N b_{mn}^N(\varphi, \mathbf{x}) \varphi_n \right) \right\|_{L^2(\Omega)}^2 \\
&\quad + \lambda^3 \left( \| e^{\lambda r^{-\beta}} (\partial_{\nu} u_m - f_m - \theta \partial_{\nu} h_m) \|_{L^2(\partial\Omega)}^2 - \| e^{\lambda r^{-\beta}} (\partial_{\nu} u_m - f_m) \|_{L^2(\partial\Omega)}^2 \right) \\
&\quad \left. + \epsilon \left( \| u_m - \theta h_m \|_{H^s(\Omega)}^2 - \| u_m \|_{H^s(\Omega)}^2 \right) \right].
\end{aligned}$$

Expanding each square and letting  $\theta \rightarrow 0^+$ , we obtain

$$\begin{aligned}
&\sum_{m=0}^N \left[ \operatorname{Re} \left\langle e^{2\lambda r^{-\beta}} \left( i \sum_{n=0}^N s_{mn} u_n + \Delta u_m + \sum_{n=0}^N b_{mn}^N(\varphi, \mathbf{x}) \varphi_n \right), i \sum_{n=0}^N s_{mn} h_n + \Delta h_m \right\rangle_{L^2(\Omega)} \right. \\
&\quad \left. + \lambda^3 \operatorname{Re} \langle e^{2\lambda r^{-\beta}} (\partial_{\nu} u_m - f_m), \partial_{\nu} h_m \rangle_{L^2(\partial\Omega)} + \epsilon \operatorname{Re} \langle u_m, h_m \rangle_{H^s(\Omega)} \right] \leq 0. \quad (4.4)
\end{aligned}$$

Similarly, interchanging the roles of  $\mathbf{u}$  and  $\mathbf{v}$ , we obtain

$$\begin{aligned}
&\sum_{m=0}^N \left[ \operatorname{Re} \left\langle e^{2\lambda r^{-\beta}} \left( i \sum_{n=0}^N s_{mn} v_n + \Delta v_m + \sum_{n=0}^N b_{mn}^N(\psi, \mathbf{x}) \psi_n \right), i \sum_{n=0}^N s_{mn} h_n + \Delta h_m \right\rangle_{L^2(\Omega)} \right. \\
&\quad \left. + \lambda^3 \operatorname{Re} \langle e^{2\lambda r^{-\beta}} (\partial_{\nu} v_m - f_m), \partial_{\nu} h_m \rangle_{L^2(\partial\Omega)} + \epsilon \operatorname{Re} \langle v_m, h_m \rangle_{H^s(\Omega)} \right] \geq 0. \quad (4.5)
\end{aligned}$$

Subtracting (4.5) from (4.4), we obtain

$$\begin{aligned}
&\sum_{m=0}^N \left[ \operatorname{Re} \left\langle e^{2\lambda r^{-\beta}} \left( i \sum_{n=0}^N s_{mn} h_n + \Delta h_m + \sum_{n=0}^N b_{mn}^N(\varphi, \mathbf{x}) \varphi_n - \sum_{n=0}^N b_{mn}^N(\psi, \mathbf{x}) \psi_n \right), \right. \right. \\
&\quad \left. \left. i \sum_{n=0}^N s_{mn} h_n + \Delta h_m \right\rangle_{L^2(\Omega)} + \lambda^3 \int_{\partial\Omega} e^{2\lambda r^{-\beta}} |\partial_{\nu} h_m|^2 d\sigma(\mathbf{x}) + \epsilon \|h_m\|_{H^s(\Omega)}^2 \right] \leq 0. \quad (4.6)
\end{aligned}$$

Rearranging (4.6) and moving the frozen nonlinear term to the right-hand side, we obtain

$$\begin{aligned}
&\sum_{m=0}^N \left[ \int_{\Omega} e^{2\lambda r^{-\beta}} \left| i \sum_{n=0}^N s_{mn} h_n + \Delta h_m \right|^2 d\mathbf{x} + \lambda^3 \int_{\partial\Omega} e^{2\lambda r^{-\beta}} |\partial_{\nu} h_m|^2 d\sigma(\mathbf{x}) + \epsilon \|h_m\|_{H^s(\Omega)}^2 \right] \\
&\leq - \sum_{m=0}^N \operatorname{Re} \left\langle e^{2\lambda r^{-\beta}} \left( \sum_{n=0}^N b_{mn}^N(\varphi, \mathbf{x}) \varphi_n - \sum_{n=0}^N b_{mn}^N(\psi, \mathbf{x}) \psi_n \right), i \sum_{n=0}^N s_{mn} h_n + \Delta h_m \right\rangle_{L^2(\Omega)}. \quad (4.7)
\end{aligned}$$

Applying the inequality  $ab \leq \frac{1}{2}(a^2 + b^2)$  to the right-hand side of (4.7), we obtain

$$\begin{aligned} & \sum_{m=0}^N \left[ \int_{\Omega} e^{2\lambda r^{-\beta}} \left| i \sum_{n=0}^N s_{mn} h_n + \Delta h_m \right|^2 d\mathbf{x} + 2\lambda^3 \int_{\partial\Omega} e^{2\lambda r^{-\beta}} |\partial_{\nu} h_m|^2 d\sigma(\mathbf{x}) + 2\epsilon \|h_m\|_{H^s(\Omega)}^2 \right] \\ & \leq \sum_{m=0}^N \int_{\Omega} e^{2\lambda r^{-\beta}} \left| \sum_{n=0}^N b_{mn}^N(\boldsymbol{\varphi}, \mathbf{x}) \varphi_n - \sum_{n=0}^N b_{mn}^N(\boldsymbol{\psi}, \mathbf{x}) \psi_n \right|^2 d\mathbf{x} \quad (4.8) \end{aligned}$$

Since  $H$  is bounded in  $[L^{\infty}(\Omega)]^{N+1}$ , the map

$$\zeta \mapsto \sum_{n=0}^N b_{mn}^N(\zeta, \mathbf{x}) \zeta_n$$

is locally Lipschitz on  $H$ , uniformly in  $\mathbf{x} \in \Omega$ . Hence,

$$\left| \sum_{n=0}^N b_{mn}^N(\boldsymbol{\varphi}, \mathbf{x}) \varphi_n - \sum_{n=0}^N b_{mn}^N(\boldsymbol{\psi}, \mathbf{x}) \psi_n \right| \leq C |\boldsymbol{\varphi}(\mathbf{x}) - \boldsymbol{\psi}(\mathbf{x})|.$$

It follows from (4.8) that

$$\begin{aligned} & \sum_{m=0}^N \left[ \int_{\Omega} e^{2\lambda r^{-\beta}} \left| i \sum_{n=0}^N s_{mn} h_n + \Delta h_m \right|^2 d\mathbf{x} + 2\lambda^3 \int_{\partial\Omega} e^{2\lambda r^{-\beta}} |\partial_{\nu} h_m|^2 d\sigma(\mathbf{x}) + 2\epsilon \|h_m\|_{H^s(\Omega)}^2 \right] \\ & \leq C \int_{\Omega} e^{2\lambda r^{-\beta}} |\boldsymbol{\varphi} - \boldsymbol{\psi}|^2 d\mathbf{x}. \quad (4.9) \end{aligned}$$

Using the inequality  $|a - b|^2 \geq \frac{1}{2}|a|^2 - |b|^2$  gives

$$\begin{aligned} & \sum_{m=0}^N \left[ \frac{1}{2} \int_{\Omega} e^{2\lambda r^{-\beta}} |\Delta h_m|^2 d\mathbf{x} - C \int_{\Omega} e^{2\lambda r^{-\beta}} |h_m|^2 d\mathbf{x} \right. \\ & \quad \left. + 2\lambda^3 \int_{\partial\Omega} e^{2\lambda r^{-\beta}} |\partial_{\nu} h_m|^2 d\sigma(\mathbf{x}) + 2\epsilon \|h_m\|_{H^s(\Omega)}^2 \right] \leq C \int_{\Omega} e^{2\lambda r^{-\beta}} |\boldsymbol{\varphi} - \boldsymbol{\psi}|^2 d\mathbf{x}. \quad (4.10) \end{aligned}$$

By applying the Carleman estimate (2.8) with  $u = h_m$ , we find

$$\begin{aligned} & \int_{\Omega} e^{2\lambda r^{-\beta}} |\Delta h_m|^2 d\mathbf{x} \\ & \geq C \int_{\Omega} e^{2\lambda r^{-\beta}} [\lambda^3 |h_m|^2 + \lambda |\nabla h_m|^2] d\mathbf{x} - C\lambda \int_{\partial\Omega} e^{2\lambda r^{-\beta}} |\partial_{\nu} h_m|^2 d\sigma(\mathbf{x}). \quad (4.11) \end{aligned}$$

Combining (4.10) and (4.11) gives

$$\begin{aligned} & \lambda^3 \int_{\Omega} e^{2\lambda r^{-\beta}} |\mathbf{h}|^2 d\mathbf{x} \\ & + 2\lambda^3 \int_{\partial\Omega} e^{2\lambda r^{-\beta}} |\partial_{\nu} \mathbf{h}|^2 d\sigma(\mathbf{x}) + 2\epsilon \|\mathbf{h}\|_{[H^s(\Omega)]^{N+1}}^2 \leq C \int_{\Omega} e^{2\lambda r^{-\beta}} |\boldsymbol{\varphi} - \boldsymbol{\psi}|^2 d\mathbf{x}. \quad (4.12) \end{aligned}$$

Add the nonlinear term

$$2C \int_{\partial\Omega} e^{2\lambda r^{-\beta}} |\partial_\nu(\varphi - \psi)|^2 d\sigma(\mathbf{x}) + \frac{2C\epsilon}{\lambda^3} \|\varphi - \psi\|_{[H^s(\Omega)]^{N+1}}^2$$

into the right hand side of (4.12) and recall  $\mathbf{h} = \mathbf{u} - \mathbf{v}$ . We obtain

$$\begin{aligned} & \lambda^3 \left[ \int_{\Omega} e^{2\lambda r^{-\beta}} |\mathbf{u} - \mathbf{v}|^2 d\mathbf{x} + 2 \int_{\partial\Omega} e^{2\lambda r^{-\beta}} |\partial_\nu(\mathbf{u} - \mathbf{v})|^2 d\sigma(\mathbf{x}) + \frac{2\epsilon}{\lambda^3} \|\mathbf{u} - \mathbf{v}\|_{[H^s(\Omega)]^{N+1}}^2 \right. \\ & \left. \leq C \left[ \int_{\Omega} e^{2\lambda r^{-\beta}} |\varphi - \psi|^2 d\mathbf{x} + 2 \int_{\partial\Omega} e^{2\lambda r^{-\beta}} |\partial_\nu(\varphi - \psi)|^2 d\sigma(\mathbf{x}) + \frac{2\epsilon}{\lambda^3} \|\varphi - \psi\|_{[H^s(\Omega)]^{N+1}}^2 \right]. \right. \end{aligned} \quad (4.13)$$

Estimate (4.3) follows.  $\square$

**Corollary 4.1.** *Let  $\epsilon > 0$ , and let  $\lambda \geq \lambda_1$ , where  $\lambda_1$  is as in Theorem 4.1. For an arbitrary initial guess  $\mathbf{u}^{(0)} \in H$ , define the Picard iteration*

$$\mathbf{u}^{(k+1)} = F_{\lambda,\epsilon}(\mathbf{u}^{(k)}), \quad k = 0, 1, 2, \dots$$

*Then the sequence  $\{\mathbf{u}^{(k)}\}_{k=0}^\infty$  converges in  $(H, \|\cdot\|_{\lambda,\epsilon})$  to a unique fixed point  $\mathbf{u}_{\lambda,\epsilon} \in H$  satisfying*

$$F_{\lambda,\epsilon}(\mathbf{u}_{\lambda,\epsilon}) = \mathbf{u}_{\lambda,\epsilon}.$$

*More precisely,  $\mathbf{u}_{\lambda,\epsilon}$  is the unique minimizer of the functional  $J_{\mathbf{u}_{\lambda,\epsilon}}^{\lambda,\epsilon}$  over the admissible set  $H$ .*

*In addition, if  $\mu \in (0, 1)$  denotes the contraction constant of  $F_{\lambda,\epsilon}$ , then*

$$\|\mathbf{u}^{(k)} - \mathbf{u}_{\lambda,\epsilon}\|_{\lambda,\epsilon} \leq \mu^k \|\mathbf{u}^{(0)} - \mathbf{u}_{\lambda,\epsilon}\|_{\lambda,\epsilon}, \quad k \geq 0.$$

*Proof.* By Theorem 4.1, the map  $F_{\lambda,\epsilon} : H \rightarrow H$  is contractive with respect to the norm  $\|\cdot\|_{\lambda,\epsilon}$ . Since  $H$  is a closed subset of  $[H^s(\Omega)]^{N+1}$  and the norm  $\|\cdot\|_{\lambda,\epsilon}$  is equivalent to the norm of  $[H^s(\Omega)]^{N+1}$ , the metric space  $(H, \|\cdot\|_{\lambda,\epsilon})$  is complete. Therefore, the conclusion follows from the Banach fixed-point theorem.  $\square$

## 5 The consistency of the fixed-point

In inverse problems, it is essential to address noisy data. If the boundary measurement  $f(\mathbf{x}, t)$ ,  $(\mathbf{x}, t) \in \partial\Omega \times (0, T)$ , in (1.2) is contaminated by noise, then the induced boundary data  $f_m$ ,  $m = 0, \dots, N$ , in (3.13) are also noisy. Let  $f_m^*$ ,  $m = 0, \dots, N$ , denote the corresponding exact data. Let  $\mathbf{u}^* = [u_0 \ \dots, u_N]^\top$  be the solution of the time-dimensional reduction model associated with the exact data, that is,  $\mathbf{u}^*$  solves

$$\begin{cases} i \sum_{n=0}^N s_{mn} u_n^*(\mathbf{x}) + \Delta u_m^*(\mathbf{x}) + \sum_{n=0}^N b_{mn}^N(\mathbf{u}^*, \mathbf{x}) u_n^*(\mathbf{x}) = 0, & \mathbf{x} \in \Omega, \\ u_m^*(\mathbf{x}) = 0, & \mathbf{x} \in \partial\Omega, \\ \partial_\nu u_m^*(\mathbf{x}) = f_m^*(\mathbf{x}), & \mathbf{x} \in \partial\Omega, \end{cases} \quad m = 0, 1, \dots, N. \quad (5.1)$$

In this section, we show that the fixed point  $\mathbf{u}_{\lambda,\epsilon}$  is close to  $\mathbf{u}^*$ . Writing  $\mathbf{f}^* = [f_0^* \ \dots, f_N^*]^\top$  and  $\mathbf{f} = [f_0 \ \dots, f_N]^\top$ , we have the theorem.

**Theorem 5.1.** Assume that  $\mathbf{u}^* \in H$  solves the exact reduced system (5.1). Let  $\mathbf{u}_{\lambda,\epsilon} \in H$  be the fixed point associated with the noisy data  $\mathbf{f} = (f_0, \dots, f_N)^\top$ , and let  $\mathbf{f}^* = (f_0^*, \dots, f_N^*)^\top$  denote the exact data. Fix  $\epsilon > 0$  and  $\beta \geq \beta_0$ . Then there exist  $\lambda_1 \geq \lambda_0$  and  $C > 0$ , depending only on  $\Omega$ ,  $\beta$ ,  $s$ ,  $N$ ,  $p$ ,  $T$ ,  $\|q\|_{L^\infty(\Omega \times (0,T))}$ ,  $\{\Psi_\ell\}_{\ell=0}^N$ ,  $\{s_{mn}\}_{m,n=0}^N$ , and  $M$ , such that for all  $\lambda \geq \lambda_1$ ,

$$\|\mathbf{u}_{\lambda,\epsilon} - \mathbf{u}^*\|_{\lambda,\epsilon}^2 \leq C \frac{\epsilon}{\lambda^3} \|\mathbf{u}^*\|_{[H^s(\Omega)]^{N+1}}^2 + C \int_{\partial\Omega} e^{2\lambda r^{-\beta}} |\mathbf{f} - \mathbf{f}^*|^2 d\sigma(\mathbf{x}). \quad (5.2)$$

*Proof.* Set

$$\mathbf{h} := \mathbf{u}_{\lambda,\epsilon} - \mathbf{u}^* = [h_0 \quad \dots \quad h_N]^\top.$$

Since  $\mathbf{u}^* \in H$  and  $H$  is convex, the same argument used to derive (4.4) yields

$$\begin{aligned} & \sum_{m=0}^N \left[ \operatorname{Re} \left\langle e^{2\lambda r^{-\beta}} \left( i \sum_{n=0}^N s_{mn} u_{\lambda,\epsilon,n} + \Delta u_{\lambda,\epsilon,m} + \sum_{n=0}^N b_{mn}^N(\mathbf{u}_{\lambda,\epsilon}, \mathbf{x}) u_{\lambda,\epsilon,n} \right), i \sum_{n=0}^N s_{mn} h_n + \Delta h_m \right\rangle_{L^2(\Omega)} \right. \\ & \quad \left. + \lambda^3 \operatorname{Re} \left\langle e^{2\lambda r^{-\beta}} (\partial_\nu u_{\lambda,\epsilon,m} - f_m), \partial_\nu h_m \right\rangle_{L^2(\partial\Omega)} + \epsilon \operatorname{Re} \langle u_{\lambda,\epsilon,m}, h_m \rangle_{H^s(\Omega)} \right] \leq 0. \quad (5.3) \end{aligned}$$

Using  $u_{\lambda,\epsilon,m} = u_m^* + h_m$  and the fact that  $\mathbf{u}^*$  solves (5.1), we obtain

$$\begin{aligned} & \sum_{m=0}^N \left[ \int_{\Omega} e^{2\lambda r^{-\beta}} \left| i \sum_{n=0}^N s_{mn} h_n + \Delta h_m \right|^2 d\mathbf{x} + \lambda^3 \int_{\partial\Omega} e^{2\lambda r^{-\beta}} |\partial_\nu h_m|^2 d\sigma(\mathbf{x}) + \epsilon \|h_m\|_{H^s(\Omega)}^2 \right] \\ & \leq - \sum_{m=0}^N \operatorname{Re} \left\langle e^{2\lambda r^{-\beta}} \left( \sum_{n=0}^N b_{mn}^N(\mathbf{u}_{\lambda,\epsilon}, \mathbf{x}) u_{\lambda,\epsilon,n} - \sum_{n=0}^N b_{mn}^N(\mathbf{u}^*, \mathbf{x}) u_n^* \right), i \sum_{n=0}^N s_{mn} h_n + \Delta h_m \right\rangle_{L^2(\Omega)} \\ & \quad - \lambda^3 \sum_{m=0}^N \operatorname{Re} \left\langle e^{2\lambda r^{-\beta}} (f_m^* - f_m), \partial_\nu h_m \right\rangle_{L^2(\partial\Omega)} - \epsilon \sum_{m=0}^N \operatorname{Re} \langle u_m^*, h_m \rangle_{H^s(\Omega)}. \quad (5.4) \end{aligned}$$

We now estimate the three terms on the right-hand side of (5.4). Since  $H$  is bounded in  $[L^\infty(\Omega)]^{N+1}$ , the map

$$\zeta \mapsto \sum_{n=0}^N b_{mn}^N(\zeta, \mathbf{x}) \zeta_n$$

is locally Lipschitz on  $H$ , uniformly in  $\mathbf{x} \in \Omega$ . Hence

$$\left| \sum_{n=0}^N b_{mn}^N(\mathbf{u}_{\lambda,\epsilon}, \mathbf{x}) u_{\lambda,\epsilon,n} - \sum_{n=0}^N b_{mn}^N(\mathbf{u}^*, \mathbf{x}) u_n^* \right| \leq C |\mathbf{h}(\mathbf{x})|.$$

Therefore, by  $ab \leq \frac{1}{2}(a^2 + b^2)$ ,

$$\begin{aligned} & \left| \operatorname{Re} \left\langle e^{2\lambda r^{-\beta}} \left( \sum_{n=0}^N b_{mn}^N(\mathbf{u}_{\lambda,\epsilon}, \mathbf{x}) u_{\lambda,\epsilon,n} - \sum_{n=0}^N b_{mn}^N(\mathbf{u}^*, \mathbf{x}) u_n^* \right), i \sum_{n=0}^N s_{mn} h_n + \Delta h_m \right\rangle_{L^2(\Omega)} \right| \\ & \leq \frac{1}{2} \int_{\Omega} e^{2\lambda r^{-\beta}} \left| i \sum_{n=0}^N s_{mn} h_n + \Delta h_m \right|^2 d\mathbf{x} + C \int_{\Omega} e^{2\lambda r^{-\beta}} |\mathbf{h}|^2 d\mathbf{x}. \quad (5.5) \end{aligned}$$

Similarly,

$$\begin{aligned} & \lambda^3 \left| \operatorname{Re} \left\langle e^{2\lambda r^{-\beta}} (f_m^* - f_m), \partial_\nu h_m \right\rangle_{L^2(\partial\Omega)} \right| \\ & \leq \frac{\lambda^3}{2} \int_{\partial\Omega} e^{2\lambda r^{-\beta}} |\partial_\nu h_m|^2 d\sigma(\mathbf{x}) + \frac{\lambda^3}{2} \int_{\partial\Omega} e^{2\lambda r^{-\beta}} |f_m - f_m^*|^2 d\sigma(\mathbf{x}), \end{aligned} \quad (5.6)$$

and

$$\epsilon \left| \operatorname{Re} \langle u_m^*, h_m \rangle_{H^s(\Omega)} \right| \leq \frac{\epsilon}{2} \|h_m\|_{H^s(\Omega)}^2 + \frac{\epsilon}{2} \|u_m^*\|_{H^s(\Omega)}^2. \quad (5.7)$$

Substituting (5.5)–(5.7) into (5.4) and absorbing the half terms into the left-hand side, we obtain

$$\begin{aligned} & \sum_{m=0}^N \left[ \int_{\Omega} e^{2\lambda r^{-\beta}} \left| i \sum_{n=0}^N s_{mn} h_n + \Delta h_m \right|^2 d\mathbf{x} + \lambda^3 \int_{\partial\Omega} e^{2\lambda r^{-\beta}} |\partial_\nu h_m|^2 d\sigma(\mathbf{x}) + \epsilon \|h_m\|_{H^s(\Omega)}^2 \right] \\ & \leq C \int_{\Omega} e^{2\lambda r^{-\beta}} |\mathbf{h}|^2 d\mathbf{x} + C\lambda^3 \int_{\partial\Omega} e^{2\lambda r^{-\beta}} |\mathbf{f} - \mathbf{f}^*|^2 d\sigma(\mathbf{x}) + C\epsilon \|u^*\|_{[H^s(\Omega)]^{N+1}}^2. \end{aligned} \quad (5.8)$$

Next, using

$$|a + b|^2 \geq \frac{1}{2}|a|^2 - |b|^2$$

with

$$a = \Delta h_m, \quad b = i \sum_{n=0}^N s_{mn} h_n,$$

we obtain

$$\left| i \sum_{n=0}^N s_{mn} h_n + \Delta h_m \right|^2 \geq \frac{1}{2} |\Delta h_m|^2 - C |\mathbf{h}|^2.$$

Hence (5.8) implies

$$\begin{aligned} & \sum_{m=0}^N \left[ \frac{1}{2} \int_{\Omega} e^{2\lambda r^{-\beta}} |\Delta h_m|^2 d\mathbf{x} + \lambda^3 \int_{\partial\Omega} e^{2\lambda r^{-\beta}} |\partial_\nu h_m|^2 d\sigma(\mathbf{x}) + \epsilon \|h_m\|_{H^s(\Omega)}^2 \right] \\ & \leq C \int_{\Omega} e^{2\lambda r^{-\beta}} |\mathbf{h}|^2 d\mathbf{x} + C\lambda^3 \int_{\partial\Omega} e^{2\lambda r^{-\beta}} |\mathbf{f} - \mathbf{f}^*|^2 d\sigma(\mathbf{x}) + C\epsilon \|u^*\|_{[H^s(\Omega)]^{N+1}}^2. \end{aligned} \quad (5.9)$$

Since both  $\mathbf{u}_{\lambda, \epsilon}$  and  $\mathbf{u}^*$  satisfy the homogeneous Dirichlet boundary condition, we have  $h_m = 0$  on  $\partial\Omega$ . Therefore, applying the Carleman estimate (2.8) to each  $h_m$ , we get

$$\int_{\Omega} e^{2\lambda r^{-\beta}} |\Delta h_m|^2 d\mathbf{x} \geq C \int_{\Omega} e^{2\lambda r^{-\beta}} (\lambda^3 |h_m|^2 + \lambda |\nabla h_m|^2) d\mathbf{x} - C\lambda \int_{\partial\Omega} e^{2\lambda r^{-\beta}} |\partial_\nu h_m|^2 d\sigma(\mathbf{x}). \quad (5.10)$$

Substituting (5.10) into (5.9), we obtain

$$\begin{aligned} & \sum_{m=0}^N \left[ C \int_{\Omega} e^{2\lambda r^{-\beta}} (\lambda^3 |h_m|^2 + \lambda |\nabla h_m|^2) d\mathbf{x} - C\lambda \int_{\partial\Omega} e^{2\lambda r^{-\beta}} |\partial_\nu h_m|^2 d\sigma(\mathbf{x}) \right. \\ & \quad \left. + \lambda^3 \int_{\partial\Omega} e^{2\lambda r^{-\beta}} |\partial_\nu h_m|^2 d\sigma(\mathbf{x}) + \epsilon \|h_m\|_{H^s(\Omega)}^2 \right] \\ & \leq C \int_{\Omega} e^{2\lambda r^{-\beta}} |\mathbf{h}|^2 d\mathbf{x} + C\lambda^3 \int_{\partial\Omega} e^{2\lambda r^{-\beta}} |\mathbf{f} - \mathbf{f}^*|^2 d\sigma(\mathbf{x}) + C\epsilon \|u^*\|_{[H^s(\Omega)]^{N+1}}^2. \end{aligned} \quad (5.11)$$

Choosing  $\lambda$  sufficiently large, we absorb the lower-order bulk term on the right-hand side and the  $C\lambda$  boundary term on the left into the corresponding  $\lambda^3$  terms. Consequently,

$$\begin{aligned} \lambda^3 \int_{\Omega} e^{2\lambda r^{-\beta}} |\mathbf{h}|^2 d\mathbf{x} + \lambda^3 \int_{\partial\Omega} e^{2\lambda r^{-\beta}} |\partial_{\nu} \mathbf{h}|^2 d\sigma(\mathbf{x}) + \epsilon \|\mathbf{h}\|_{[H^s(\Omega)]^{N+1}}^2 \\ \leq C\lambda^3 \int_{\partial\Omega} e^{2\lambda r^{-\beta}} |\mathbf{f} - \mathbf{f}^*|^2 d\sigma(\mathbf{x}) + C\epsilon \|\mathbf{u}^*\|_{[H^s(\Omega)]^{N+1}}^2. \end{aligned} \quad (5.12)$$

Dividing by  $\lambda^3$  yields

$$\begin{aligned} \int_{\Omega} e^{2\lambda r^{-\beta}} |\mathbf{h}|^2 d\mathbf{x} + \int_{\partial\Omega} e^{2\lambda r^{-\beta}} |\partial_{\nu} \mathbf{h}|^2 d\sigma(\mathbf{x}) + \frac{\epsilon}{\lambda^3} \|\mathbf{h}\|_{[H^s(\Omega)]^{N+1}}^2 \\ \leq C \int_{\partial\Omega} e^{2\lambda r^{-\beta}} |\mathbf{f} - \mathbf{f}^*|^2 d\sigma(\mathbf{x}) + C \frac{\epsilon}{\lambda^3} \|\mathbf{u}^*\|_{[H^s(\Omega)]^{N+1}}^2. \end{aligned} \quad (5.13)$$

By the definition of  $\|\cdot\|_{\lambda, \epsilon}$  and after adjusting the constant  $C$ , (5.2) follows.  $\square$

**Remark 5.1.** We note that the exact modal vector  $\mathbf{u}^* = (u_0^*, \dots, u_N^*)^\top$  should be understood as the exact solution of the truncated reduced model. If instead  $\mathbf{u}^*$  is taken to be the first  $N+1$  modes of the exact solution  $u$  of the original nonlinear Schrödinger equation, then  $\mathbf{u}^*$  satisfies the truncated system only up to a truncation residual:

$$i \sum_{n=0}^N s_{mn} u_n^*(\mathbf{x}) + \Delta u_m^*(\mathbf{x}) + \sum_{n=0}^N b_{mn}^N(\mathbf{u}^*, \mathbf{x}) u_n^*(\mathbf{x}) = R_m^N(\mathbf{x}), \quad m = 0, \dots, N.$$

Here  $R_m^N$  represents the contribution of the discarded modes and the error caused by replacing the full nonlinear term by its  $N$ -mode approximation. If

$$u \in H^\ell((0, T); H^s(\Omega)), \quad \ell \geq 3, \quad s > \frac{d}{2} + 2,$$

then the Legendre-polynomial-exponential expansion of  $u$  converges in  $L^2((0, T); H^s(\Omega))$ . Hence the tail

$$u(\mathbf{x}, t) - \sum_{\ell=0}^N u_\ell^*(\mathbf{x}) \Psi_\ell(t)$$

converges to 0 in  $L^2((0, T); H^s(\Omega))$  as  $N \rightarrow \infty$ . Since  $H^s(\Omega) \hookrightarrow L^\infty(\Omega)$  and the nonlinear map  $z \mapsto |z|^{p-1}z$  is locally Lipschitz on bounded subsets of  $\mathbb{C}$ , the truncation error in the nonlinear term also converges to 0. Therefore, for each fixed  $m \geq 0$ ,

$$\int_{\Omega} e^{2\lambda r^{-\beta}} |R_m^N(\mathbf{x})|^2 d\mathbf{x} \rightarrow 0 \quad \text{as } N \rightarrow \infty.$$

Thus  $R_m^N$  is precisely the residual caused by replacing the full projected system by its  $N$ -mode truncation.

**Remark 5.2.** Fix the Carleman parameters  $\lambda$ ,  $\beta$ , and  $\mathbf{x}_0$ . Then estimate (5.2) shows that if the boundary data  $\mathbf{f}$  are close to the exact data  $\mathbf{f}^*$ , the fixed point  $\mathbf{u}_{\lambda, \epsilon}$  provides an approximation of the exact reduced solution  $\mathbf{u}^*$ . More precisely, the reconstruction error is controlled by two terms: the data discrepancy term  $\int_{\partial\Omega} e^{2\lambda r^{-\beta}} |\mathbf{f} - \mathbf{f}^*|^2 d\sigma(\mathbf{x})$ , and the regularization term  $\frac{\epsilon}{\lambda^3} \|\mathbf{u}^*\|_{[H^s(\Omega)]^{N+1}}^2$ . Therefore, for fixed Carleman parameters and small  $\epsilon$ , if  $\mathbf{f} \rightarrow \mathbf{f}^*$ , then  $\mathbf{u}_{\lambda, \epsilon}$  is close to  $\mathbf{u}^*$  in the norm  $\|\cdot\|_{\lambda, \epsilon}$ .

**Remark 5.3.** *There is no contradiction between the ill-posedness of the original inverse initial-data problem and the stability estimate in Theorem 5.1. Indeed, the theorem does not assert stability for the full inverse problem in its original infinite-dimensional form. Instead, we first approximate that problem by the time-dimensional reduction model (3.13), which is obtained by truncating the Legendre polynomial-exponential expansion to the first  $N + 1$  modes. This truncation removes the high-oscillation components of the solution, which are typically the most sensitive to noise, and therefore acts as a filtering mechanism. After this reduction, we solve a regularized problem for the coupled elliptic system with Cauchy data by means of the weighted functional  $J_\varphi^{\lambda, \epsilon}$ . The resulting fixed point  $\mathbf{u}_{\lambda, \epsilon}$  is thus the solution of a stabilized and finite-dimensional approximation of the original inverse problem. The stability estimate in Theorem 5.1 should be understood in this regularized sense.*

## 6 Numerical study

In this section, we present the numerical study for solving Problem 1.1, including the Carleman contraction method in Algorithm 1, and show some numerical results.

### 6.1 Forward problem and data generation

In this subsection, we describe the numerical procedure used to generate synthetic data for the inverse problem. The forward solution is computed on the square domain  $\Omega := (-R, R)^2$  with  $R = 1$ . We use a uniform Cartesian grid in space and a uniform partition in time. More precisely, we set

$$N_x = 61, \quad x_i = -R + (i - 1)h_x, \quad y_j = -R + (j - 1)h_y,$$

for  $i, j = 1, \dots, N_x$ , where

$$h_x = h_y = \frac{2R}{N_x - 1}.$$

In time, we choose

$$\Delta t = 1.25 \times 10^{-4}, \quad T = 0.2,$$

and define

$$t_n = n\Delta t, \quad n = 0, 1, \dots, N_t,$$

where  $N_t = T/\Delta t$ .

To generate the synthetic data, we solve the forward nonlinear Schrödinger equation with  $q(\mathbf{x}, t) = 1$  (for simplicity)

$$\begin{cases} iu_t + \Delta u + |u|^{p-1}u = 0, & (\mathbf{x}, t) \in \Omega \times (0, T), \\ u(\mathbf{x}, t) = 0, & (\mathbf{x}, t) \in \partial\Omega \times (0, T), \\ u(\mathbf{x}, 0) = u^{0, \text{true}}(\mathbf{x}), & \mathbf{x} \in \Omega, \end{cases} \quad (6.1)$$

where  $u^{0, \text{true}}$  is the prescribed exact initial condition. In all computations, the boundary condition is homogeneous Dirichlet. Although the theoretical analysis is carried out for a general coefficient  $q = q(\mathbf{x}, t)$ , in the numerical experiments we restrict ourselves to the representative case  $q \equiv 1$  for simplicity of implementation. This choice allows us to isolate the performance of the reconstruction method without reducing the scope of the analytical results.

---

**Algorithm 1** Reconstruction of the initial wave field via the Carleman–Picard iteration
 

---

- 1: Fix the artificial parameters  $\lambda$ ,  $\beta$ ,  $\mathbf{x}_0$ ,  $\epsilon$ , and the truncation number  $N$ .
- 2: Construct the Legendre polynomial-exponential basis  $\{\Psi_n\}_{n=0}^N$  and compute the projected boundary data

$$f_m(\mathbf{x}) = \int_0^T e^{-2t} f(\mathbf{x}, t) \Psi_m(t) dt, \quad m = 0, \dots, N.$$

- 3: Choose an initial guess

$$\mathbf{u}^{(0)} = \left[ u_0^{(0)} \quad u_1^{(0)} \quad \dots \quad u_N^{(0)} \right]^\top \in H.$$

- 4: **for**  $k = 0, 1, 2, \dots, K_{\max} - 1$  (for some  $K_{\max} \geq 1$ ) **do**
- 5:   For the frozen coefficient vector  $\mathbf{u}^{(k)}$ , compute  $\mathbf{u}^{(k+1)} \in H$  as the unique minimizer of

$$J_{\mathbf{u}^{(k)}}^{\lambda, \epsilon}(\mathbf{u}).$$

Equivalently,

$$\mathbf{u}^{(k+1)} = F_{\lambda, \epsilon}(\mathbf{u}^{(k)}).$$

- 6: **end for**
- 7: Set the computed coefficient vector as

$$\mathbf{u}^{\text{comp}} = \mathbf{u}^{(K_{\max})}.$$

- 8: Write

$$\mathbf{u}^{\text{comp}} = \left[ u_0^{\text{comp}} \quad \dots \quad u_N^{\text{comp}} \right]^\top$$

and reconstruct the approximate space-time solution by

$$u^{\text{comp}}(\mathbf{x}, t) := \sum_{n=0}^N u_n^{\text{comp}}(\mathbf{x}) \Psi_n(t).$$

- 9: Compute the approximate solution of the inverse problem, namely the initial wave field,

$$u^{\text{comp}}(\mathbf{x}, 0) = \sum_{n=0}^N u_n^{\text{comp}}(\mathbf{x}) \Psi_n(0).$$


---

We discretize (6.1) by a semi-implicit scheme in which the Laplacian is treated implicitly while the nonlinear term is evaluated explicitly at the previous time level. Let  $u^n$  denote the numerical approximation of  $u(\cdot, t_n)$ . Then, for  $n = 0, 1, \dots, N_t - 1$ , we compute  $u^{n+1}$  from

$$i \frac{u^{n+1} - u^n}{\Delta t} + \Delta_h u^{n+1} + |u^n|^{p-1} u^n = 0,$$

where  $\Delta_h$  is the standard five-point finite difference approximation of the Laplacian,

$$(\Delta_h u)_{i,j} = \frac{u_{i+1,j} - 2u_{i,j} + u_{i-1,j}}{h_x^2} + \frac{u_{i,j+1} - 2u_{i,j} + u_{i,j-1}}{h_y^2}.$$

At each time step, this scheme yields a linear system for  $u^{n+1}$ . The homogeneous Dirichlet boundary condition is enforced by setting the boundary values of  $u^{n+1}$  equal to zero.

After solving the forward problem, we compute the boundary observation

$$f^*(\mathbf{x}, t) = \partial_\nu u(\mathbf{x}, t) \quad \text{for } (\mathbf{x}, t) \in \partial\Omega \times (0, T),$$

by finite differences on the boundary. The noisy data are defined by

$$f^\delta(\mathbf{x}, t) = f^*(\mathbf{x}, t)(1 + \delta \text{rand}(\mathbf{x}, t)),$$

where  $\delta = 10\%$  and  $\text{rand}(\mathbf{x}, t)$  is a complex-valued random function uniformly distributed in the unit disk, satisfying  $|\text{rand}(\mathbf{x}, t)| \leq 1$  for all  $(\mathbf{x}, t)$ .

The projected data used in the reduced inverse model are then obtained by

$$f_m^\delta(\mathbf{x}) = \int_0^T e^{-2t} f^\delta(\mathbf{x}, t) \Psi_m(t) dt, \quad m = 0, \dots, N.$$

These quantities serve as the exact boundary inputs in the time-dimensional reduction model.

## 6.2 Implementation

In this subsection, we discuss several implementation details used in our numerical computations.

In Step 1, the artificial parameters are selected by manual tuning. More precisely, we adjust the parameters  $\lambda$ ,  $\beta$ ,  $\mathbf{x}_0$ ,  $\epsilon$ , and  $N$  until satisfactory numerical performance is obtained for a reference experiment, namely Test 1. In our implementation, we use  $N = 65$ ,  $\epsilon = 10^{-6}$ , and  $K_{\max} = 10$ . For the Carleman weight, we choose  $\lambda = 20$ ,  $\beta = 5$ , and  $\mathbf{x}_0 = (0, 8)$ . Once these parameters are determined from Test 1, the same values are used for all remaining tests.

In Step 3, we choose the initial guess  $\mathbf{u}^{(0)} = \mathbf{0} \in H$ .

We now discuss the implementation in Step 5. At the  $k$ th Picard step, given the current iterate  $\mathbf{u}^{(k)}$ , we first evaluate the frozen nonlinear term

$$\sum_{n=0}^N b_{mn}^N(\mathbf{u}^{(k)}, \mathbf{x}) u_n^{(k)}(\mathbf{x}), \quad m = 0, \dots, N,$$

and then keep this term fixed in the reduced system. This leads to a linear weighted least-squares problem for the next iterate  $\mathbf{u}^{(k+1)}$ . More precisely,  $\mathbf{u}^{(k+1)}$  is computed by minimizing the functional  $J_{\mathbf{u}^{(k)}}^{\lambda, \epsilon}$ , which consists of the weighted residual of the frozen reduced equations, the Neumann boundary mismatch term, and the Sobolev regularization term. In the MATLAB implementation, this minimization problem is assembled as an overdetermined linear system of the form  $A\mathbf{x} \approx \mathbf{b}$ , where  $A$  is the system matrix,  $\mathbf{x}$  is the vector of unknown discrete values of the coefficients  $u_0, \dots, u_N$ , and  $\mathbf{b}$  is the corresponding right-hand side vector. We then solve this system by the MATLAB command  $\mathbf{x} = A \setminus \mathbf{b}$ , which returns the least-squares solution. Repeating this procedure for  $k = 0, 1, 2, \dots$  generates the sequence  $\{\mathbf{u}^{(k)}\}_{k \geq 0}$ , whose last iterate is taken as the computed approximation of the fixed point  $\mathbf{u}_{\lambda, \epsilon}$ .

**Remark 6.1.** *We note that the theoretical minimization problem is posed over the admissible set  $H$ , which includes the a priori bound  $\|\mathbf{u}\|_{[L^\infty(\Omega)]^{N+1}} \leq M$ . This constraint is used in the analysis to guarantee that the nonlinear modal map is Lipschitz on the admissible set and hence to prove the contraction property of  $F_{\lambda, \epsilon}$ . In the numerical implementation, however, we solve the linear least-squares problem obtained at each Picard step by the unconstrained MATLAB command  $A \setminus \mathbf{b}$ . This is a practical implementation of the Carleman–Picard iteration. In all numerical tests reported below, the computed iterates remained uniformly bounded and the Dirichlet boundary condition was imposed directly on the discrete unknowns. Thus the computed solutions stayed inside a bounded discrete analogue of the admissible set.*

All other steps in Algorithm 1, including the projection of the boundary data and the reconstruction of the space-time solution and the initial data, are straightforward to implement once the coefficient vectors have been computed.

### 6.3 Numerical examples

In this subsection, we present some numerical tests obtained by Algorithm 1.

**Test 1.** For Test 1, we choose the true initial wave field in the form

$$u^0(x, y) = u_R^0(x, y) + i u_I^0(x, y),$$

where the real and imaginary parts are two spatially separated disk-shaped inclusions. More precisely,

$$u_R^0(x, y) = \begin{cases} 1, & (x + 0.25)^2 + (y - 0.15)^2 < 0.18^2, \\ 0, & \text{otherwise,} \end{cases}$$

and

$$u_I^0(x, y) = \begin{cases} 1.5, & (x - 0.20)^2 + (y + 0.20)^2 < 0.24^2, \\ 0, & \text{otherwise.} \end{cases}$$

Thus,  $u^0$  consists of a real-valued circular inclusion centered at  $(-0.25, 0.15)$  with radius 0.18, and an imaginary-valued circular inclusion centered at  $(0.20, -0.20)$  with radius 0.24 and amplitude 1.5. In this test, we choose  $p = 2$ , corresponding to a quadratic power-type nonlinearity.

Figure 1 shows that the proposed method remains effective even in the presence of 10% noise in the boundary data. Visually, both inclusions are reconstructed at the correct locations, and their supports are captured well. The real part is recovered near  $(-0.25, 0.15)$ , while the imaginary part is clearly identified near  $(0.20, -0.20)$ . The Picard iteration is also numerically stable: the relative change decreases steadily, and the dimensionless residual decays monotonically to a small level, indicating convergence of the algorithm. Quantitatively, the maximum value of the reconstructed real part is 1.048345, compared with the true amplitude 1, which corresponds to a relative amplitude error of 4.83%. For the imaginary part, the reconstructed maximum is 1.351354, compared with the true amplitude 1.5, giving a relative amplitude error of 9.91%. Thus, despite the presence of 10% noise, the method still yields accurate reconstructions of both the geometry and the amplitudes of the two inclusions.

To quantify the convergence of the Picard iteration, we use the relative change and the dimensionless residual, which are displayed in Figures 1c and 1f, respectively. The relative change at the  $k$ th Picard iteration is defined by

$$\text{RelChange}^{(k)} := \frac{\|\mathbf{U}^{(k+1)} - \mathbf{U}^{(k)}\|_{[L^2(\Omega)]^{N+1}}}{\|\mathbf{U}^{(k+1)}\|_{[L^2(\Omega)]^{N+1}}}, \quad (6.2)$$

where

$$\mathbf{U}^{(k)} = \left( u_0^{(k)}, u_1^{(k)}, \dots, u_N^{(k)} \right)^\top$$

denotes the vector of modal coefficients at the  $k$ th iteration. We also define the dimensionless residual by

$$\text{Res}^{(k)} := \frac{\|iS\mathbf{U}^{(k)} + \Delta\mathbf{U}^{(k)} + \mathbf{B}(\mathbf{U}^{(k)})\|_{[L^2(\Omega)]^{N+1}}}{\max \left\{ \|\Delta\mathbf{U}^{(k)}\|_{[L^2(\Omega)]^{N+1}}, 10^{-2} \right\}} \quad (6.3)$$

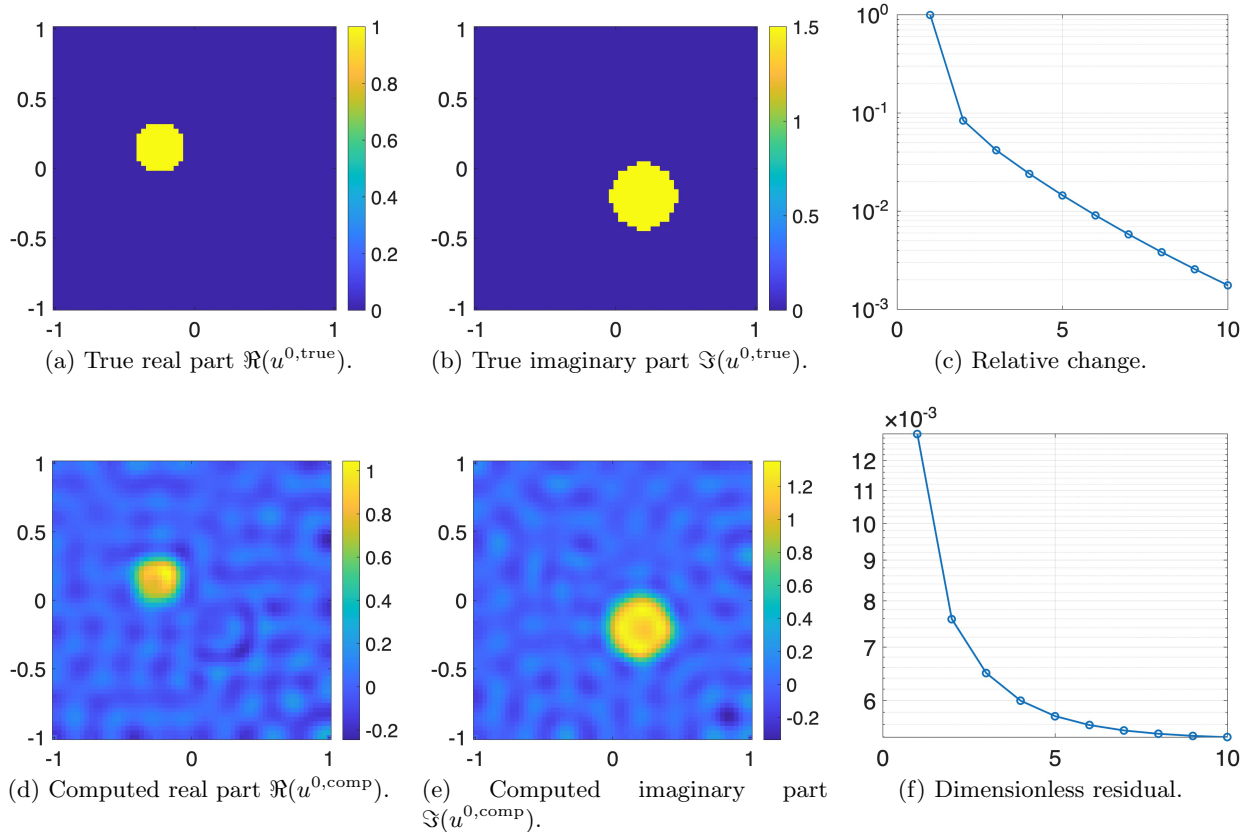


Figure 1: Test 1. Top row: true real and imaginary parts of the initial wave field, together with the relative change versus the Picard iteration. Bottom row: computed real and imaginary parts, together with the dimensionless residual versus the Picard iteration.

where

$$\mathbf{B}(\mathbf{U}^{(k)})(\mathbf{x}) := \left( \int_0^T e^{-2t} q(\mathbf{x}, t) \left| \sum_{\ell=0}^N u_{\ell}^{(k)}(\mathbf{x}) \Psi_{\ell}(t) \right|^{p-1} \left( \sum_{\ell=0}^N u_{\ell}^{(k)}(\mathbf{x}) \Psi_{\ell}(t) \right) \Psi_m(t) dt \right)_{m=0}^N.$$

The normalization in the definition of  $\text{Res}^{(k)}$  makes the residual dimensionless and avoids division by a very small quantity.

**Test 2.** For Test 2, we choose the true initial wave field in the form

$$u^0(x, y) = u_R^0(x, y) + i u_I^0(x, y),$$

where the real and imaginary parts are defined by simple geometric inclusions. More precisely, the real part consists of two disk-shaped inclusions of amplitude 2:

$$u_R^0(x, y) = \begin{cases} 2, & (x + 0.35)^2 + (y - 0.15)^2 < 0.30^2, \\ 0, & \text{otherwise,} \end{cases} + \begin{cases} 2, & (x - 0.30)^2 + (y + 0.25)^2 < 0.30^2, \\ 0, & \text{otherwise.} \end{cases}$$

The imaginary part is a square ring of amplitude 2, centered at  $(0.05, 0.05)$ , with outer half-width 0.60 and inner half-width 0.42:

$$u_I^0(x, y) = \begin{cases} 2, & \max\{|x - 0.05|, |y - 0.05|\} < 0.60 \text{ and } \max\{|x - 0.05|, |y - 0.05|\} \geq 0.42, \\ 0, & \text{otherwise.} \end{cases}$$

Thus, the real part contains two separated circular inclusions, while the imaginary part is supported on a square annulus. In this test, we set  $p = 3$ , so that the model becomes the cubic nonlinear Schrödinger equation, which arises in important applications including nonlinear optics and Bose–Einstein condensates.

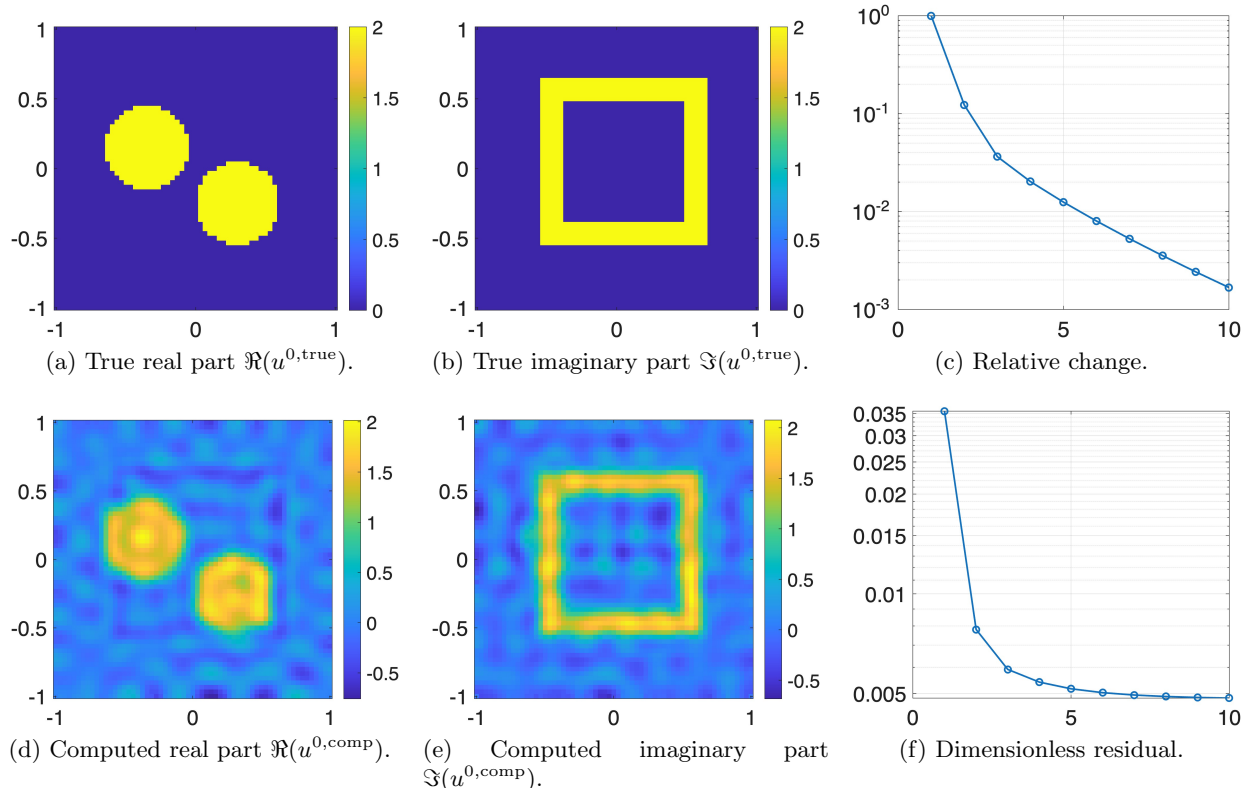


Figure 2: Test 2. Top row: true real and imaginary parts of the initial wave field, together with the relative change versus the Picard iteration. Bottom row: computed real and imaginary parts, together with the dimensionless residual versus the Picard iteration.

The numerical results for Test 2 are displayed in Figure 2. They show that the proposed method performs very well in this more complicated setting. Visually, the two disk-shaped inclusions in the real part are accurately recovered, with the correct locations, sizes, and amplitudes. The square-ring structure in the imaginary part is also reconstructed clearly, and its geometric shape is well preserved, although a mild background oscillation is still visible in the computed images. The convergence of the Picard iteration is confirmed by the quantities defined in (6.2) and (6.3): the relative change decreases rapidly and monotonically over the iterations, while the dimensionless residual also decays to a small level, indicating that the iterates stabilize and that the reduced nonlinear system is satisfied with increasing accuracy. Quantitatively, the maximum value of the reconstructed real part is 2.015303, compared with the true amplitude 2, which corresponds to a relative amplitude error of 0.76515%. For the imaginary part, the reconstructed maximum is 2.077241, compared with the true amplitude 2, giving a relative amplitude error of 3.86205%. These results show that the method can recover both the geometry and the amplitudes of the true initial wave field with high accuracy.

**Test 3.** For Test 3, we choose the true initial wave field in the form

$$u^0(x, y) = u_R^0(x, y) + i u_I^0(x, y),$$

where the real and imaginary parts have different geometric structures. The real part is an annulus centered at the origin:

$$u_R^0(x, y) = \begin{cases} 1, & 0.24 \leq \sqrt{x^2 + y^2} \leq 0.52, \\ 0, & \text{otherwise.} \end{cases}$$

The imaginary part is chosen in the shape of the letter N, and is defined as

$$u_I^0(x, y) = \begin{cases} 1, & -0.42 \leq x \leq -0.24, -0.42 \leq y \leq 0.42, \\ 1, & 0.20 \leq x \leq 0.38, -0.42 \leq y \leq 0.42, \\ 1, & |y + 1.55x + 0.06| \leq 0.10, -0.30 \leq x \leq 0.26, -0.42 \leq y \leq 0.42, \\ 0, & \text{otherwise.} \end{cases}$$

Thus, the real part is supported on a circular ring, while the imaginary part consists of two vertical bars connected by a diagonal strip, forming an N-shaped inclusion. In this test we choose  $p = 5$ , corresponding to a quintic nonlinear Schrödinger model, which is relevant in certain settings involving higher-order nonlinear effects.

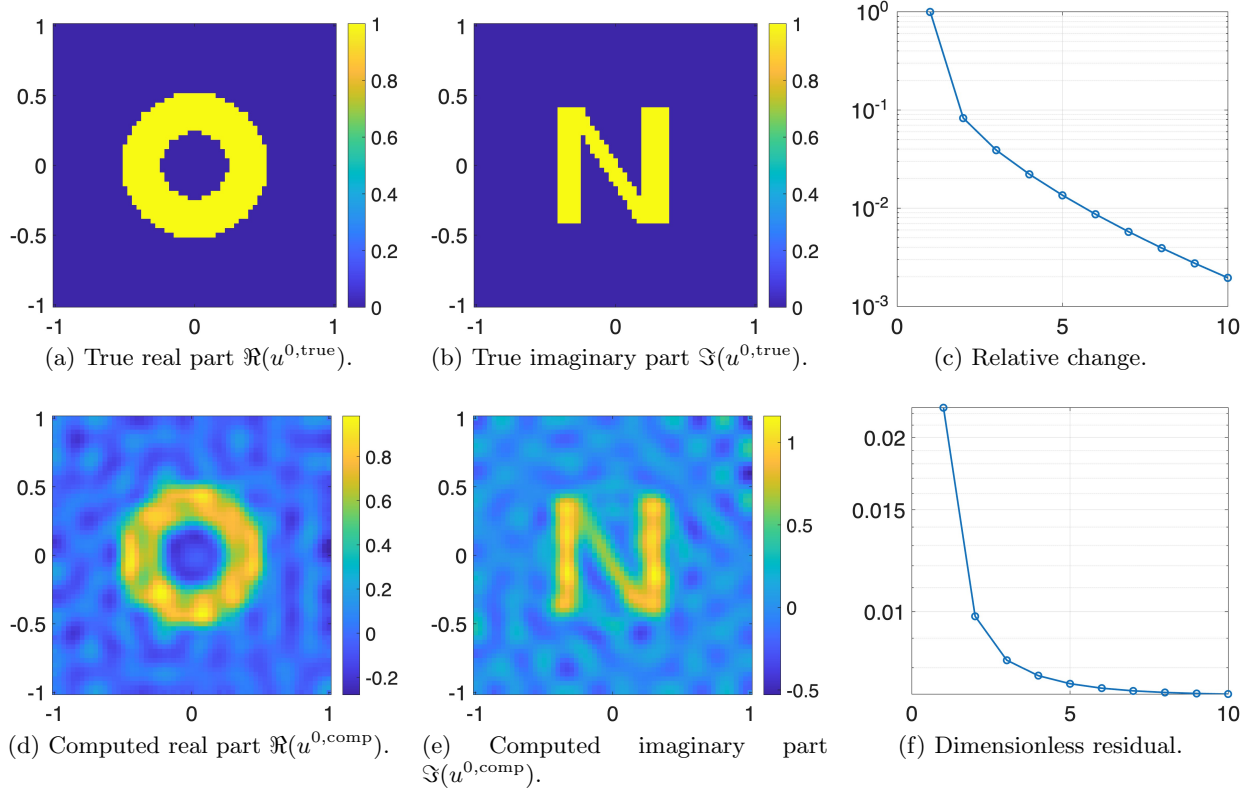


Figure 3: Test 3. Top row: true real and imaginary parts of the initial wave field, together with the relative change versus the Picard iteration. Bottom row: computed real and imaginary parts, together with the dimensionless residual versus the Picard iteration.

The numerical results for Test 3 are shown in Figure 3. They indicate that the proposed method performs well even for this more intricate geometry. Visually, the annular structure in the real part is clearly recovered, with the correct location, thickness, and circular shape. The N-shaped inclusion in the imaginary part is also reconstructed successfully: the two vertical bars and the connecting diagonal segment are all visible and match the true profile well. The convergence of the Picard iteration is stable, as evidenced by the steady decay of both the relative change and the dimensionless residual throughout the iterations. Quantitatively, the maximum value of the reconstructed real part is 0.9835456, compared with the true amplitude 1, which corresponds to a relative amplitude error of 1.65%. For the imaginary part, the reconstructed maximum is 1.159482, compared with the true amplitude 1, giving a relative amplitude error of 15.95%. Overall, the method accurately captures the main geometric features of both components and exhibits robust convergence in this quintic case.

**Remark 6.2.** *For all three numerical tests, the reconstruction results are very good, despite a noise level of 10% in the boundary data. In particular, the proposed method remains stable across different geometries and different nonlinear exponents, while still recovering the main shapes, locations, and amplitudes of the true initial wave fields with good accuracy. These numerical experiments indicate that the Carleman–Picard method is both effective and robust in the presence of substantial measurement noise.*

**Remark 6.3.** *In this paper, we set  $\Psi_n(t) = e^t Q_n(t)$ , where  $\{Q_n\}_{n \geq 0}$  are the shifted Legendre polynomials on  $(0, T)$ . Although the factor  $e^t$  is canceled by the weight  $e^{-2t}$  in the inner product of  $L^2_{e^{-2t}}(0, T)$ , it becomes essential when time derivatives appear. Indeed,*

$$\Psi'_n(t) = \frac{d}{dt}(e^t Q_n(t)) = e^t(Q_n(t) + Q'_n(t)),$$

which is not identically zero on  $(0, T)$ . Therefore, in the expansion (3.2), namely,

$$u_t(\mathbf{x}, t) = \sum_{n=0}^{\infty} u_n(\mathbf{x}) \Psi'_n(t),$$

every coefficient  $u_n(\mathbf{x})$  contributes to the time derivative, and this contribution is retained in the reduced system (3.13).

By contrast, if one uses the standard shifted Legendre basis  $\{Q_n\}_{n \geq 0}$  without the exponential factor, then the lowest mode satisfies  $Q'_0(t) = 0$  for all  $t$ , since  $Q_0$  is constant. As a consequence, the corresponding coefficient  $u_0(\mathbf{x})$  does not appear in the derivative expansion through the term involving  $Q'_0$ , which may weaken the coupling between modes and lead to a loss of information in the time-reduced model. The exponential factor avoids this difficulty by ensuring that even the lowest time mode remains visible in the differentiated expansion.

## 6.4 Comparison with a Direct Unsupervised PINN Baseline

For comparison, we also implemented a direct unsupervised physics-informed neural network (PINN) baseline for the original inverse problem (1.1)–(1.2), without using the Legendre polynomial-exponential time-dimensional reduction and Carleman weight functions. In this approach, the neural network directly approximates the complex-valued wave field

$$u(\mathbf{x}, t) = u_R(\mathbf{x}, t) + i u_I(\mathbf{x}, t), \quad (\mathbf{x}, t) \in \Omega \times (0, T),$$

where  $u_R$  and  $u_I$  denote the real and imaginary parts, respectively. The input of the network is the three-dimensional variable  $(x, y, t)$ , and the output consists of the two real-valued components  $u_R(x, y, t)$  and  $u_I(x, y, t)$ .

The network is a fully connected feedforward neural network with six hidden layers, each of width 256. Its architecture is

$$3 \rightarrow 256 \rightarrow 256 \rightarrow 256 \rightarrow 256 \rightarrow 256 \rightarrow 256 \rightarrow 2,$$

where the input dimension 3 corresponds to  $(x, y, t)$  and the output dimension 2 corresponds to  $(u_R, u_I)$ . The activation function in every hidden layer is tanh, so that the network is sufficiently smooth for automatic differentiation of the first- and second-order derivatives appearing in the Schrödinger equation.

The PINN is trained by minimizing a loss function consisting of three parts: the residual of the nonlinear Schrödinger equation in the interior of  $\Omega \times (0, T)$ , the homogeneous Dirichlet boundary condition on  $\partial\Omega \times (0, T)$ , and the measured Neumann boundary data on  $\partial\Omega \times (0, T)$ . The total loss is defined by

$$\mathcal{L}(\theta) = \omega_{\text{int}}\mathcal{L}_{\text{int}}(\theta) + \omega_{\text{D}}\mathcal{L}_{\text{D}}(\theta) + \omega_{\text{N}}\mathcal{L}_{\text{N}}(\theta),$$

where, in our implementation,

$$\omega_{\text{int}} = 1, \quad \omega_{\text{D}} = 20, \quad \omega_{\text{N}} = 20.$$

These weights are selected by manual tuning so as to achieve satisfactory numerical results. The interior residual loss is given by

$$\mathcal{L}_{\text{int}}(\theta) = \frac{1}{N_{\text{int}}} \sum_{j=1}^{N_{\text{int}}} \left| i \partial_t u_\theta(\mathbf{x}_j, t_j) + \Delta u_\theta(\mathbf{x}_j, t_j) + q(\mathbf{x}_j, t_j) |u_\theta(\mathbf{x}_j, t_j)|^{p-1} u_\theta(\mathbf{x}_j, t_j) \right|^2,$$

the Dirichlet boundary loss is

$$\mathcal{L}_{\text{D}}(\theta) = \frac{1}{N_{\text{D}}} \sum_{j=1}^{N_{\text{D}}} |u_\theta(\mathbf{x}_j, t_j)|^2,$$

and the Neumann boundary loss is

$$\mathcal{L}_{\text{N}}(\theta) = \frac{1}{N_{\text{N}}} \sum_{j=1}^{N_{\text{N}}} |\partial_\nu u_\theta(\mathbf{x}_j, t_j) - f(\mathbf{x}_j, t_j)|^2.$$

Here,  $u_\theta$  denotes the network output associated with the parameter vector  $\theta$ .

All spatial and temporal derivatives are computed by automatic differentiation. The network is trained using the Adam optimizer. In our implementation, the learning rate is set to  $10^{-3}$ , the number of training epochs is 4000, and the collocation batch sizes are 1024 for interior points, 512 for Dirichlet boundary points, and 512 for Neumann boundary points. After training, the reconstructed initial wave field is obtained by evaluating the trained network at time  $t = 0$ , namely,

$$u^{0, \text{comp}}(\mathbf{x}) = u_\theta(\mathbf{x}, 0).$$

As shown in Figure 4, for the data from Test 1, the direct unsupervised PINN baseline is able to recover the approximate locations of both inclusions. In particular, the imaginary part is reconstructed at roughly the correct location and with the correct qualitative shape. However, the recovered real part still contains visible artifacts, including a spurious negative region, and the

amplitudes are not captured as accurately as those produced by the proposed method. By contrast, the Carleman–Picard method yields reconstructions with more accurate geometry and amplitude for the same test. Therefore, for the present inverse problem and under our implementation, the Carleman–Picard method appears to be more effective than the direct unsupervised PINN baseline. This comparison is intended only as an illustrative baseline, rather than a comprehensive benchmark against optimized PINN methods. Nevertheless, the PINN experiment is still informative, since it shows that residual-based neural-network training can recover meaningful qualitative features of the inclusions.

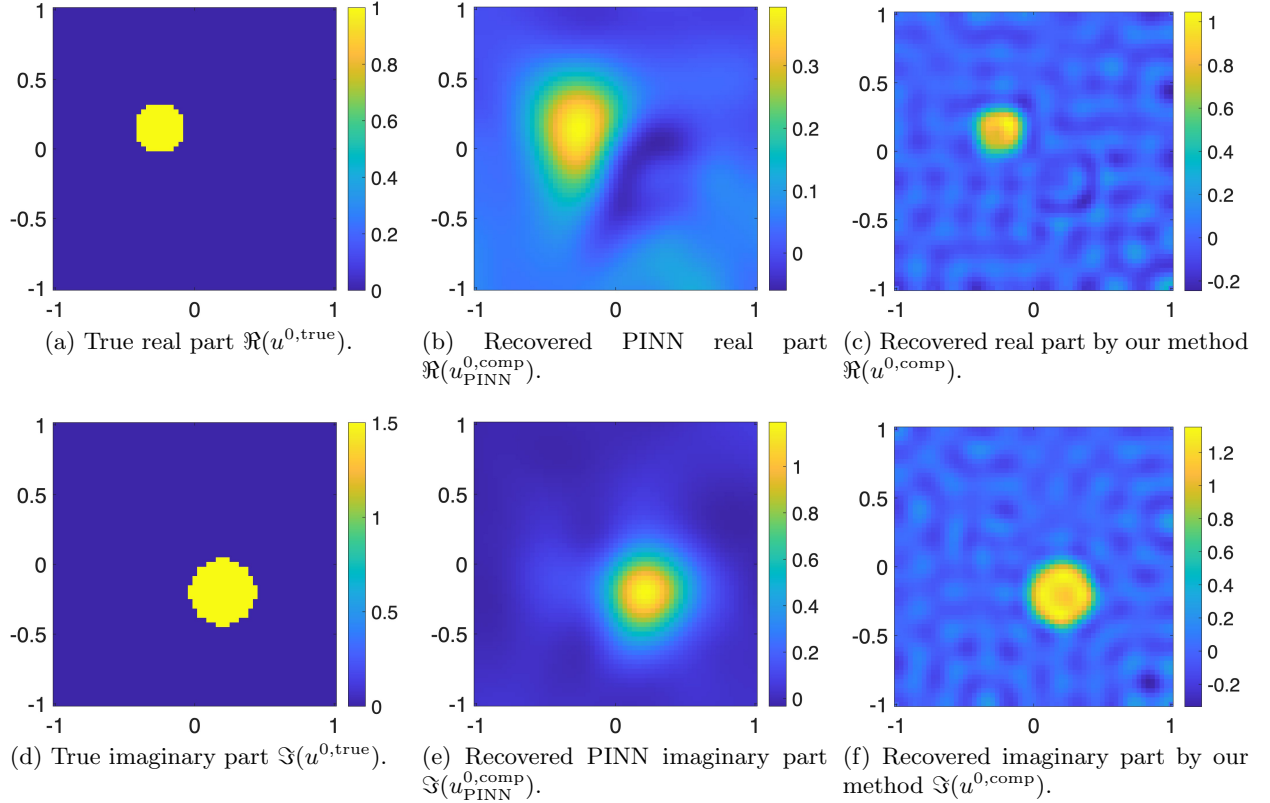


Figure 4: Comparison of reconstructions for Test 1. The second column shows the result of the direct unsupervised PINN baseline, while the third column shows the reconstruction produced by the proposed Carleman–Picard method.

## 7 Concluding remarks

In this paper, we studied an inverse initial-data problem for a nonlinear Schrödinger equation with lateral Neumann measurements. The main idea was to combine a Legendre-polynomial-exponential-time dimensional reduction with a Carleman-based contraction principle. This approach transforms the original inverse problem into a reduced nonlinear elliptic system for the time-expansion coefficients, and then solves that system using a globally convergent Picard iteration.

On the theoretical side, we constructed a contraction map on a suitable admissible set and proved that its unique fixed point is consistent with the exact reduced solution. We also established a stability estimate in the noisy-data case. In particular, the error bound does not require any

special structural assumption on the noise, which distinguishes the present framework from several standard Carleman-based approaches.

On the numerical side, we proposed a practical reconstruction algorithm and tested it on several examples with different geometries and nonlinear exponents. The numerical results show that the method is stable and accurate, even when the data contain a significant level of noise. We also presented a comparison with a direct unsupervised PINN baseline. In our numerical experiments, that approach was able to recover some qualitative features of the inclusions, but the proposed Carleman–Picard method produced more accurate reconstructions.

## References

- [1] Ray Abney, Thuy T. Le, Loc H. Nguyen, and Cam Peters. A Carleman-Picard approach for reconstructing zero-order coefficients in parabolic equations with limited data. *Applied Mathematics and Computation*, 494:129286, 2025.
- [2] Pranav Arrepu and Hanming Zhou. Stable determination of coefficients in nonlinear dynamical Schrödinger equations by Carleman estimates. Preprint, arXiv:2508.07231, 2025.
- [3] Lucie Baudouin and Alberto Mercado. An inverse problem for Schrödinger equations with discontinuous main coefficient. *Applicable Analysis*, 87(10–11):1145–1165, 2008.
- [4] Larisa Beilina and Michael V. Klibanov. *Approximate Global Convergence and Adaptivity for Coefficient Inverse Problems*. Springer, New York, 2012.
- [5] Mourad Bellassoued and Oumaima Ben Fraj. Stability estimates for time-dependent coefficients appearing in the magnetic Schrödinger equation from arbitrary boundary measurements. *Inverse Problems and Imaging*, 14(5):841–865, 2020.
- [6] Mourad Bellassoued and Mourad Choulli. Logarithmic stability in the dynamical inverse problem for the Schrödinger equation by arbitrary boundary observation. *Journal de Mathématiques Pures et Appliquées*, 91:233–255, 2009.
- [7] Mourad Bellassoued and Mourad Choulli. Stability estimate for an inverse problem for the magnetic Schrödinger equation from the Dirichlet-to-Neumann map. *Journal of Functional Analysis*, 258(1):161–195, 2010.
- [8] Mourad Bellassoued, Yavar Kian, and Eric Soccorsi. An inverse stability result for non-compactly supported potentials by one arbitrary lateral Neumann observation. *Journal of Differential Equations*, 260(10):7535–7562, 2016.
- [9] Mourad Bellassoued, Yavar Kian, and Eric Soccorsi. An inverse problem for the magnetic Schrödinger equation in infinite cylindrical domains. *Publications of the Research Institute for Mathematical Sciences*, 54:679–728, 2018.
- [10] Ibtissem Ben Aïcha and Yosra Mejri. Simultaneous determination of the magnetic field and the electric potential in the Schrödinger equation by a finite number of boundary observations. *Journal of Inverse and Ill-Posed Problems*, 26(2):201–209, 2018.
- [11] Alexander L. Bukhgeim and Michael V. Klibanov. Global uniqueness of a class of multidimensional inverse problems. *Soviet Mathematics Doklady*, 24:244–247, 1981.

- [12] Thierry Cazenave. *Semilinear Schrödinger Equations*, volume 10 of *Courant Lecture Notes in Mathematics*. American Mathematical Society, Providence, RI, 2003.
- [13] Mourad Choulli, Yavar Kian, and Eric Soccorsi. Stable determination of time-dependent scalar potential from boundary measurements in a periodic quantum waveguide. *SIAM Journal on Mathematical Analysis*, 47(6):4536–4558, 2015.
- [14] Michel Cristofol and Eric Soccorsi. Stability estimate in an inverse problem for non-autonomous magnetic Schrödinger equations. *Applicable Analysis*, 90(10):1499–1520, 2011.
- [15] Trong D. Dang, Loc H. Nguyen, and Huong T. T. Vu. Determining initial conditions for nonlinear hyperbolic equations with time dimensional reduction and the Carleman contraction principle. *Inverse Problems*, 40:125021, 2024.
- [16] Klaus Deimling. *Nonlinear Functional Analysis*. Springer-Verlag, Berlin, 1985.
- [17] Li Deng. An inverse problem for the Schrödinger equation with variable coefficients and lower order terms. *Journal of Mathematical Analysis and Applications*, 427(2):930–940, 2015.
- [18] Gregory Eskin. Inverse problems for the Schrödinger operators with electromagnetic potentials in domains with obstacles. *Inverse Problems*, 19(4):985–996, 2003.
- [19] Gregory Eskin. Inverse problems for the Schrödinger equations with time-dependent electromagnetic potentials and the Aharonov–Bohm effect. *Journal of Mathematical Physics*, 49(2):022105, 2008.
- [20] Xinchu Huang, Yavar Kian, Eric Soccorsi, and Masahiro Yamamoto. Carleman estimate for the Schrödinger equation and application to magnetic inverse problems. *Journal of Mathematical Analysis and Applications*, 474(1):116–142, 2019.
- [21] Oleg Yu. Imanuvilov and Masahiro Yamamoto. Lipschitz stability in inverse parabolic problems by the Carleman estimate. *Inverse Problems*, 14(5):1229–1245, 1998.
- [22] Vo Anh Khoa, Michael V. Klibanov, and Loc H. Nguyen. Convexification for a 3D inverse scattering problem with the moving point source. *SIAM Journal on Imaging Sciences*, 13(2):871–904, 2020.
- [23] Yavar Kian and Eric Soccorsi. Hölder stably determining the time-dependent electromagnetic potential of the Schrödinger equation. *SIAM Journal on Mathematical Analysis*, 51(2):627–647, 2019.
- [24] Michael V. Klibanov, Thuy T. Le, Loc H. Nguyen, Anders Sullivan, and Lam Nguyen. Convexification-based globally convergent numerical method for a 1D coefficient inverse problem with experimental data. *Inverse Problems and Imaging*, 16(6):1579–1618, 2022.
- [25] Michael V. Klibanov and Jingzhi Li. *Inverse Problems and Carleman Estimates: Global Uniqueness, Global Convergence and Experimental Data*. De Gruyter, Berlin, 2021.
- [26] Michael V. Klibanov and Loc H. Nguyen. Carleman estimates and the contraction principle for an inverse source problem for nonlinear hyperbolic equations. *Inverse Problems*, 38(3):035009, 2022.

- [27] Katsiaryna Krupchyk and Gunther Uhlmann. Inverse problems for nonlinear magnetic Schrödinger equations on conformally transversally anisotropic manifolds. *Analysis and PDE*, 16(8):1825–1868, 2023.
- [28] Ru-Yu Lai, Xuezhu Lu, and Ting Zhou. Partial data inverse problems for the nonlinear time-dependent Schrödinger equation. *SIAM Journal on Mathematical Analysis*, 56(4):4712–4741, 2024.
- [29] Ru-Yu Lai and Ting Zhou. Partial data inverse problems for nonlinear magnetic Schrödinger equations. *Mathematical Research Letters*, 30(5):1535–1563, 2023.
- [30] Robert Lattès and Jacques-Louis Lions. *The Method of Quasi-Reversibility: Applications to Partial Differential Equations*. Elsevier, New York, 1969.
- [31] Thuy T. Le. Global reconstruction of initial conditions of nonlinear parabolic equations via the Carleman-contraction method. In D-L. Nguyen, L. H. Nguyen, and T-P. Nguyen, editors, *Advances in Inverse problems for Partial Differential Equations*, volume 784 of *Contemporary Mathematics*, pages 23–42. American Mathematical Society, 2023.
- [32] Huynh P. N. Le, Thuy T. Le, and Loc H. Nguyen. The Carleman convexification method for Hamilton-Jacobi equations. *Computers and Mathematics with Applications*, 159:173–185, 2024.
- [33] Thuy T. Le, Linh V. Nguyen, Loc H. Nguyen, and Hyunha Park. The time dimensional reduction method to determine the initial conditions without the knowledge of damping coefficients. *Computers and Mathematics with Applications*, 166:77–90, 2024.
- [34] Thuy T. Le and Loc H. Nguyen. A convergent numerical method to recover the initial condition of nonlinear parabolic equations from lateral Cauchy data. *Journal of Inverse and Ill-Posed Problems*, 30(2):265–286, 2022.
- [35] Thuy T. Le, Cong B. Van, Trong D. Dang, and Loc H. Nguyen. Inverse initial data reconstruction for Maxwell’s equations via time-dimensional reduction method. Preprint, arXiv:2506.20777, 2025.
- [36] J.-H. Lee, O. K. Pashaev, C. Rogers, and W. K. Schief. The resonant nonlinear Schrödinger equation in cold plasma physics. application of Bäcklund–Darboux transformations and superposition principles. *Journal of Plasma Physics*, 73(2):257–272, 2007.
- [37] Alberto Mercado, Axel Osses, and Lionel Rosier. Inverse problems for the Schrödinger equation via Carleman inequalities with degenerate weights. *Inverse Problems*, 24(1):015017, 2008.
- [38] Dinh-Liem Nguyen, Loc H. Nguyen, and Trung Truong. The Carleman-based contraction principle to reconstruct the potential of nonlinear hyperbolic equations. *Computers and Mathematics with Applications*, 128:239–248, 2022.
- [39] Hoai-Minh Nguyen and Loc H. Nguyen. Cloaking using complementary media for the Helmholtz equation and a three spheres inequality for second order elliptic equations. *Transactions of the American Mathematical Society, Series B*, 2:93–112, 2015.
- [40] Loc H. Nguyen. An inverse space-dependent source problem for hyperbolic equations and the Lipschitz-like convergence of the quasi-reversibility method. *Inverse Problems*, 35:035007, 2019.

- [41] Loc H. Nguyen. The Carleman contraction mapping method for quasilinear elliptic equations with over-determined boundary data. *Acta Mathematica Vietnamica*, 48:401–422, 2023.
- [42] Phuong M. Nguyen and Loc H. Nguyen. A Carleman contraction method for inverse initial data recovery in the Navier–Stokes equations with unknown body force. *arXiv preprint arXiv:2604.09934*, 2026.
- [43] Phuong M. Nguyen, Loc H. Nguyen, and Huong T. Vu. Solving the inverse scattering problem via Carleman-based contraction mapping. *Computers and Mathematics with Applications*, 209:129–143, 2026.
- [44] Lev Pitaevskii and Sandro Stringari. *Bose-Einstein Condensation and Superfluidity*. Oxford University Press, 2016.
- [45] Murray H. Protter. Unique continuation for elliptic equations. *Transactions of the American Mathematical Society*, 95(1):81–91, 1960.
- [46] Abdelkarim Saci and Salah-Eddine Rebiai. An inverse problem for the Schrödinger equation with Neumann boundary condition. *Advances in Pure and Applied Mathematics*, 14(1):50–69, 2023.
- [47] Catherine Sulem and Pierre-Louis Sulem. *The Nonlinear Schrödinger Equation: Self-Focusing and Wave Collapse*. Springer, New York, 1999.
- [48] Dang D. Trong, Chanh V. Le, Khoa D. Luu, and Loc H. Nguyen. Recovery of initial displacement and velocity in anisotropic elastic systems by the time dimensional reduction method. *Journal of Computational Physics*, 542:114371, 2025.
- [49] Cong B. Van, Thuy T. Le, and Loc H. Nguyen. The inverse initial data problem for anisotropic Navier–Stokes equations via Legendre time reduction method. *Communications in Nonlinear Science and Numerical Simulation*, 161:110074, 2026.
- [50] Nikolay K. Vitanov, Amin Chabchoub, and Norbert Hoffmann. Deep-water waves: On the nonlinear Schrödinger equation and its solutions. *Journal of Theoretical and Applied Mechanics*, 43(2):169–191, 2013.
- [51] Eberhard Zeidler. *Nonlinear Functional Analysis and its Applications, Volume III: Variational Methods and Optimization*. Springer-Verlag, New York, 1985.